Analysis of elastic events at center of mass energy $\sqrt{s} = 1{,}96TeV$ and scintillating fibers efficiency at the Forward Proton Detector

David Alejandro Martinez C.

Jaime Betancourt, MSc.
Director

University of Nariño
Faculty of Natural Science and Mathematics
Physics Department
Pasto, Colombia
December 2006

Summary

In this graduate work is shown that the Forward Proton Detector located at D$\emptyset$ experiment has a good quality data sample to make measurements of the differential cross section at center of mass energy $\sqrt{s} = 1{,}96$ TeV on the interval of four momentum transfer between 0.2 t 1.5 $(GeV/c)^2$.
No other experiment has been able to make a measurement in this t range. Also different analysis techniques are developed to establish the Forward Proton Detector performance, and mainly to guarantee the existence of the elastic signal in this detector to obtain distributions of $\frac{dN}{dt}$.
Furthermore some comparisons of the results of this graduate work are made with other research institutes and investigators.

To God
To my Grandmother
To my Mother and Aunt

Acknowledgements

I would like to thank my Director, Jaime Betancourt, for helping me on this work, for giving me his friendship and to show me that experimental physics is a great research field which has excellent and interesting results. To Professor Carlos Avila because he gave us the opportunity to work in this kind of investigation, and also always help us to have a good development of the project. To the Physics Department and specially the Professors: Juan, Yithsbey, Alfredo.” Thanks Professors”.

Personal Acknowledgements

I would like to thank my grandmother Olga because she was one of the most important persons in my life. To my mother and my aunt “KATHY” because always have been here to understand me through all the years. To all my family and specially to my aunt Janetth. To my University friends: Alejandro, one of my best friends and a great person, I learn a lot of things of him “Thanks” , William and Edwin, the friends that always have been here “don’t forget the chiken and the pig”, and Oscar.

Índice general

Índice de figuras

Índice de cuadros

Introduction

Quantum chromodynamics is a very important theory used to describe and predict the strong interactions. The QCD based on the quarks model is a solid base for the understanding of structure of the matter. In the Tevatron around $25\,\%$ of the $\overline{P}P$ cross section is elastic, where the momentum exchanged is low and therefore perturbative QCD isn't able to explain these phenomena[12]. The tools that we can use to understand the elastic scattering are given by the properties of the scattering amplitude and by phenomenologycal models that describe existent experimental data and predict the behaviour of the scattering amplitude to higher energies.

Among these models the most powerful is based on Regge's theory which predicts that in an elastic scattering process an exchange of a particle called POMERON is produced. From experimental information the nature of the POMERON can be understood, one sample of data useful to understand the POMERON is from elastic collisions[12].

The experiments made to study diffractive and elastic processes at different center of mass energies correspond to energies lower than $\sqrt{s} = 1{,}96TeV$, this limit is given by the higher energy reached at the moment by the particle accelerator. The FPD(Forward Proton Detector) which is a subdetector of the $D\emptyset$ experiment at the Fermilab laboratory has been constructed to track the scattered proton and/or antiproton in an elastic and diffractive collision which presents a small scattering angle and a small fraction of momentum transfer.

The FPD is constituted by quadrupolar and dipolar spectrometers that record the positions of the protons and/or antiprotons that remain intact after the collision. The Roman Pots contain scintillating fibers which give the (X, Y) coordinates[10] of these events. The fibers are read out by multianode photomultipliers that are interfaced with the electronics of the experiment[9].

With the detector coordinates tha particle trajectory can be reconstructed. If we know the magnetic field between the interaction point and the detector location as well as the position of the detector one can determine the momentum lost (ξ) of the particle that remained intact after the collision, also one can determine the momentum transfered t and finally using these variables detailed studies of the differential cross section can be made.

This is the first experimental analysis of high energy physics made by the University of Nariño with the collaboration of the Andes University .

In this work two studies are made: one is the scintillating fibers efficiency and the other is an analysis of elastic events to confirm the existence of an elastic signal in the FPD detectors to obtain preliminary distributions of $\frac{dN}{dt}$; we work with a data sample that was taken on February 17 and 18 of 2006 that corresponds to the run numbers between 215417 and 215449.
In chapter one is shown the physical theories presented for high energy elastic collisions, for $\overline{P}P$ collisions in terms of kinematic variables, also it is presented a short summary of the latest measurements of the elastic differential cross section.
In chapter two we present the general characteristics of the Tevatron accelerator and the $D\emptyset$ detector, continuing in chapter 3 with the FPD detector and its characteristics, components, coordinate and data acquisition system. In chapter 4 we present two different forms to reconstruct the particle's trajectory from the FPD detector to the interaction point. Chapter five contains the methodology of the analysis to determine fiber efficiencies, in chapter six efficiency values are determined for all the fibers belonging to the FPD and the results obtained for fiber efficiencies are compared with results obtained by Brasilian researchers. Finally in chapter 7 a study of elastic events is made that allow us to show that an elastic physical signal exists in the detectors of the FPD and for these reason at the end we obtained good distributions of $\frac{dN}{dt}$.

Capítulo 1

1. KINEMATIC VARIABLES

In the Kinematic study of a collison it is important to use variables and appropiate reference frames. Some important concepts of the interaction kinematics will be introduced in this chapter.

1.1 SYSTEM AND VARIABLES USED ON SCATTERING

We are interested on the kinematics of scattering process of the form:

$$1 + 2 \rightarrow 3 + 4 \tag{1.1}$$

For elastic scattering:

particle 1 = particle 3 and particle 2 = particle 4

Furthemore we use the natural units $c = \hbar = \frac{h}{2\pi} = 1$

The choice of the Lorentz system depends on the system symmetry, for example useful systems are when the sum of the four-momenta is equal to zero, some of these are:

A. Laboratory frame: one of the two particles are on rest.
B. $p1 + p2$ and $p3 + p4$ cancel, Center of mass frame
C. $p1 + p3$ and $p2 + p4$ cancel

The quantities in the center of mass frame are indicated with an asterisk, while laboratory frame without asterisk.

1.2 MANDELSTAM VARIABLES

A useful set of Lorentz-invariant variables used in calculations are the Mandelstam variables **s**, **t** and **u**. These variables are defined as following:

1. Square of the center of mass energy (CMS):

$$s = (P_1 + P_2)^2 = (E_1^* + E_2^*)^2 = m_1^2 + m_2^2 + 2E_1 m_2 = (m_1 + m_2)^2 + 2T_1 m_2 \tag{1.2}$$

2. Four-momentum transfered squared between particles 1 and 3

$$t = (P_1 - P_3)^2 = m_1^2 + m_3^2 - 2E_1^* E_3^* + 2p_1^* p_3^* \cos(\theta_3^*) = m_1^2 + m_3^2 - 2E_1 E_3 + 2p_1 p_3 \cos(\theta_3) \tag{1.3}$$

$$t = (P_2 - P_4)^2 = m_2^2 + m_4^2 - 2E_2^* E_4^* + 2p_2^* p_4^* \cos(\theta_4^*) = (m_2 - m_4)^2 - 2m_2(E_4 - m_4) \tag{1.4}$$

Table 1.1 Variables for the i particle on laboratory and mass center frames

	MASS CENTER FRAME	*LABORATORY FRAME*
Momentum (3-d)	$\overrightarrow{p_i}^*$	$\overrightarrow{p_i}$
Kinetic Energy	T_i^*	T_i
Total Energy	E_i^*	E_i
Four-momenta	$\mathrm{P}_i^* = (E_i^*, \overrightarrow{p_i}^*)$	$\mathrm{P}_i = (E_i, \overrightarrow{p_i})$
Scattering angle	θ_i^*	θ_i
Rest mass	m_i	m_i
Velocity/c	β_i^*	β_i
Transversal momentum	p_t^*	p_t
For both frames	$\mathrm{P}^2 = E^2 - p^2 = m^2$	
	T = E - m	

3. Four-momentum transfered squared between particles 1 and 4

$$u = (P_1 - P_4)^2 = m_1^2 + m_4^2 - 2E_1^*E_4^* + 2p_1^*p_4^*\cos(\theta_4^*) = m_1^2 + m_4^2 - 2E_1E_4 + 2p_1p_4\cos(\theta_4) \quad (1.5)$$

$$u = (P_2 - P_3)^2 = m_2^2 + m_3^2 - 2E_2^*E_3^* + 2p_2^*p_3^*\cos(\theta_3^*) = (m_2 - m_3)^2 - 2m_2(E_3 - m_3) \quad (1.6)$$

These three variables satisfy the relation[1] :

$$s + t + u = \sum_{j=1}^{4} m_j^2 \quad (1.7)$$

For elastic scattering:

$$p_1^* = p_2^* = p_3^* = p_4^* = p^* \quad (1.8)$$

$$E_1^* = E_3^*, \quad E_2^* = E_4^* \quad (1.9)$$

Then the equations for **s**, **t**, **u** can be written[7]:

$$\begin{aligned} s &= 4(\overrightarrow{p}^2 + m^2c^2) \\ t &= -\overrightarrow{p}^2(1 - \cos\theta) \\ u &= -2\overrightarrow{p}^2(1 + \cos\theta) \end{aligned} \quad (1.10)$$

1.3 THE DIFFERENTIAL ELASTIC CROSS SECTION

Clasically the study of an incoming particle with energy E over a scattering center, with an impact parameter *b*, and a scattering angle θ, is shown in figure 1.2 The particles that

[1] F. Halzen, A. MArtin *Quarks and Leptons*, Jhon Wiley Sons, (1984).

Fig 1.1 Elastic collision of two particles

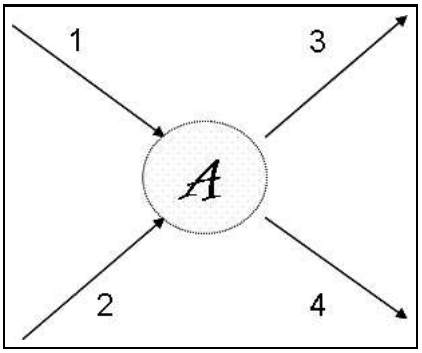

Fig 1.2.Cross Section

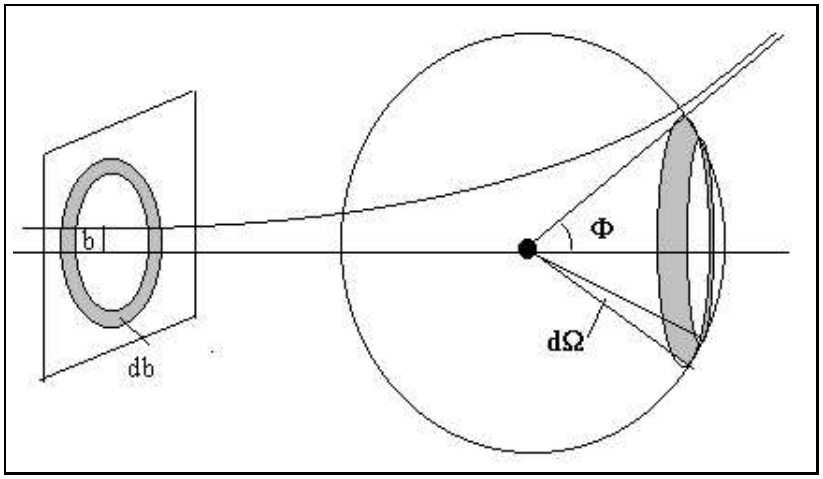

have a croos section $d\sigma$ scatter in a solid angle $d\Omega$. Clasically is given by[2]:

$$D(\Phi) = \frac{b}{\sin(\Phi)}|\frac{db}{d\Phi}| \tag{1.11}$$

In quantum theory the differential cross section with respect to the center of mass reference system is given by:

$$\frac{d\sigma}{dt} = \frac{\pi}{p^2}\frac{d\sigma}{d\Omega_{cm}} = \frac{\pi}{p^2}|f|^2 \tag{1.12}$$

Where f is the scattering amplitude and is composed by two parts for proton and antiproton elastic scattering:[3]

1. The electromagnetic amplitude or Coulomb amplitude (f_c)
2. The nuclear amplitude or Hadronic amplitude (f_n)

The Coulomb amplitude is obtained from the Rutherford equation[3] :

$$f_c = \mp\frac{2p\alpha G^2(t)}{4\pi|t|} \tag{1.13}$$

Where the sign "+" is defined for the $p\bar{p}$ interaction and "-" for the pp interaction, α is the fine structure constant $\left(\alpha = \frac{1}{137,037}\right)$ and $G(t)$ is the electromagnetic form factor of the proton and it is given by[4]:

$$G(t) \approx \left(1 + \frac{|t|}{0,71}\right)^{-2} \tag{1.14}$$

With the help of the experimental observations for $|t| < 0,1GeV^2$ it has been established the amplitude for nuclear scattering can be parametrized as[3]:

$$f_n = \frac{p\sigma_T(\rho + i)e^{(\frac{-B|t|}{2})}}{4\pi} \tag{1.15}$$

The differential cross section is related to the imaginary part of the nuclear scattering amplitude trough the optical theorem:

$$\sigma_T = \frac{4\pi}{p}Im(f_n(t = 0)) \tag{1.16}$$

Where ρ is the ratio of the real to the imaginary part of the nuclear scattering amplitude at $|t| = 0$:

$$\rho = \frac{Re(f_n(t))}{Im(f_n(t))}|_{t=0} \tag{1.17}$$

[2] J. Villamil, *Mediciones de dispersión elástica con el detector FPD en el experimento $D\emptyset$*, Proyecto de grado para optar al titulo de Físico, Universidad de los Andes, 2002.

[3] C. Avila *Measurement of the proton-antiproton total cross section at center of mass energy of 1800 GeV*, PhD, Thesis, Cornell University, 1997.

[4] The $D\emptyset$ Collaboration, *Proposal for a Forward Proton Detector at $D\emptyset$*, Fermilab-Pub-97-377, 1997.

B is the nuclear slope parameter. In general the differential cross section for $p\bar{p}$ and pp interactions can be written as:

$$d\sigma/dt = \frac{\pi}{p^2}|f_n + f_c exp(\mp i\alpha\phi(t))|^2 \tag{1.18}$$

Where $\alpha\phi(t)$ represents the phase difference between the Coulomb and Nuclear interactions and it is given by[2]:

$$\phi(t) = \ln\left(\frac{0{,}08}{|t|}\right) - 0{,}577 \tag{1.19}$$

For small values of $|t|$. Replacing the results obtained before in equation 1.18:

$$d\sigma/dt = \frac{4\pi(\hbar c)^2\alpha^2 G(t)^4}{|t|^2} \mp \frac{\alpha(\rho \mp \alpha\phi)\sigma_T G(t)^2}{|t|} exp(\frac{-B|t|}{2}) + \frac{(1+\rho^2)\sigma_T^2}{16\pi(\hbar c)^2} exp(-B|t|) \tag{1.20}$$

Where the "+" sign is for the $p\bar{p}$ interaction and "-" for the pp interaction.

Equation 1.12 is valid only for values of $|t| < |t|_{min}$ where the $|t|_{min}$ belongs to the difraction minimum. An emphirical parametrization for dσ/dt in the region beyond the minimum of difraction does not exist there are phenomenological models that predict the shapeof dσ/dt beyond the diffraction minimum, two of the models are the Block's Model[5] shown in figure 1.3 and the model of Pomeron exchange based on Regge Theory[6].

1.4 MEASUREMENTS OF THE DIFFERENTIAL ELASTIC CROSS SECTION

The differential elastic cross section for $p\bar{p}$ collisions has been measured at different center of mass energies $\sqrt{s}$ and different intervals of $|t|$, the experimental observations show different behaviors for dσ/dt depending of the interval of $|t|$, for this reason there are different $|t|$ regions that can be studied separately, in general there exists four regions at the Tevatron energy:

1. The region of $|t| < 0{,}001 GeV^2$, where the main contribution to dσ/dt is given by the Coulomb interaction and is useful for the normalization of dσ/dt.
2. The region of Nuclear-Coulomb interference for $0{,}001 < |t| < 0{,}01 GeV^2$. This is used to make measurements of the ratio of the real to the imaginary part of the scattering amplitude (ρ).
3. The region of Nuclear diffraction for $0{,}01 < |t| < 0{,}5 GeV^2$. In this region the contribution to dσ/dt is due to the strong interaction, where we dont have a theory that could explain the shape of dσ/dt of basic pronciples, for this reason dσ/dt has been parametrized emphirically. The experimental observations indicate that the best parametrization is an exponential

[5] M. Block *et al*, Phys. Rev. **D 41**, 978 (1990)

[6] P. Collins, *An Introduction to Regge Theory and High Energy Physics*, Cambridge University Press, April 28 (1977).

Fig 1.3.Block Function

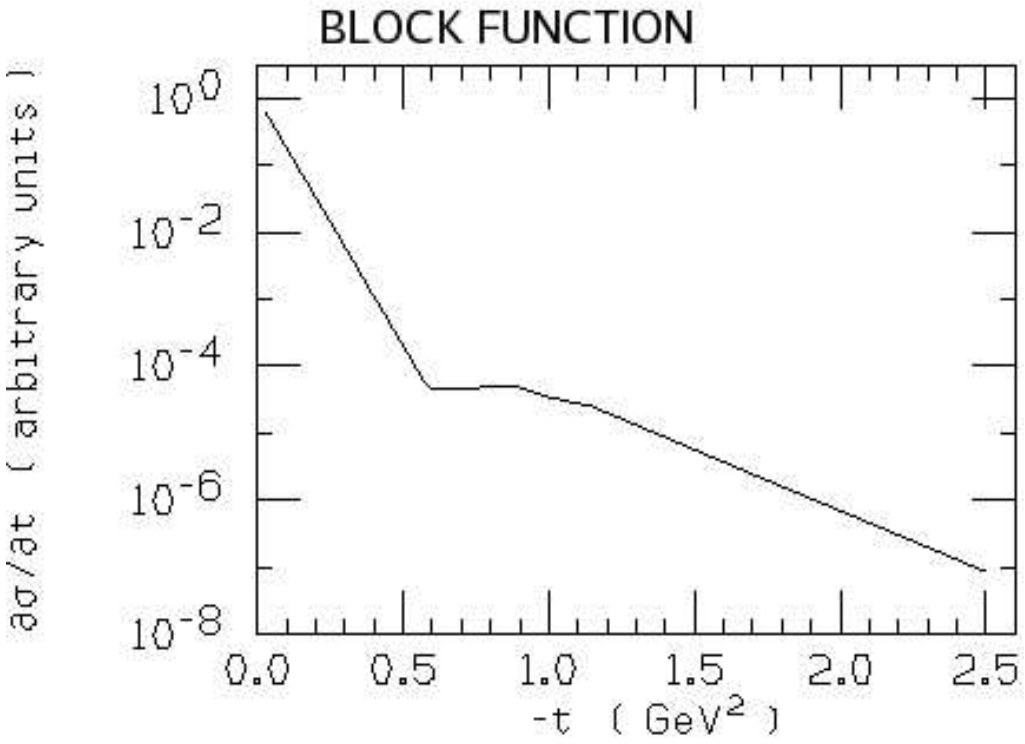

function given by: dσ/dt= $\exp(-B|t|)$, this region is important for the measurement of the total cross section(σ) and the Nuclear slope parameter B.
4. $|t| > 0{,}5GeV^2$ In this region dσ/dt presents a diffraction minimum followed by a maximum and afterwards dσ/dt has an exponential decay.

The latest experimental measurements of dσ/dt for $p\bar{p}$ interactions are:

A. CERN ISR[4] ($\sqrt{s}$=53 GeV, 1985).
B. CERN S$P\bar{P}$S[4]($\sqrt{s}$=546 GeV, 1985)
C. Fermilab[4]($\sqrt{s}$=1.8 TeV, 1994) .
D. Fermilab[7]

Figure 1.4 shows dσ/dt as a function of $|t|$ for energies of $\sqrt{s}$=53 GeV, $\sqrt{s}$=546 GeV , $\sqrt{s}$=1.8 TeV and $\sqrt{s}$=1.96 TeV, in the figure it can be observed that the diffraction minimum is moving towards lower $|t|$ values where the collision energy is increased.

1.5 LUMINOSITY

[7]J. Molina, *Estudo do espalhamento elástico em colisõnes $p\bar{p}$ a $\sqrt{s} = 1{,}96TeV$ com o Detector de Prótons Frontais FPD*, Tese Doutorado, Centro Brasileiro de Pesquisas Físicas, Rio de Janeiro, Septembro de 2003.($\sqrt{s}$=1.96 TeV, 2003)

Fig 1.4 Differential Cross Section

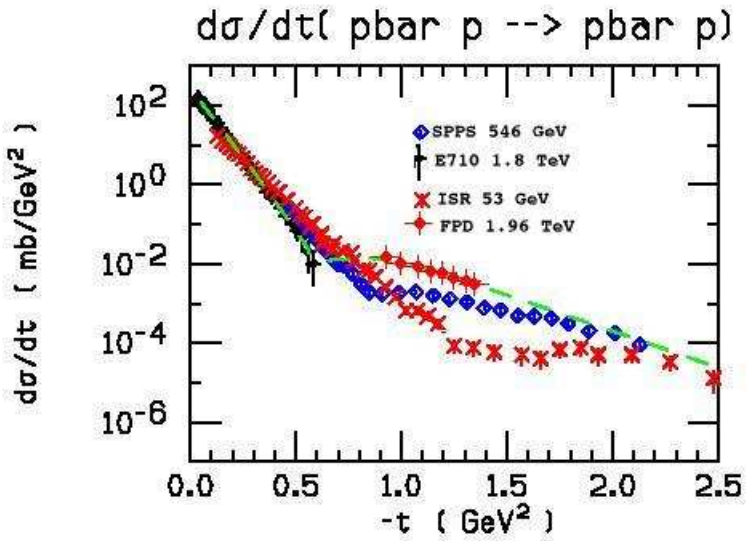

The Luminosity is defined as the number of incident particles, per unit of time per unit of area, then:

$$D(\theta) = \frac{1}{L}\frac{dN}{d\Omega} \tag{1.21}$$

In the quantum theory of scattering an incident wave of the form $\psi_i(z) = Ae^{ikz}$, travel in the *z* direction, and finds a scattering potential, and as result a spherical wave is produced $\psi_0(r) \sim A\{e^{ikz} + f(\theta)\frac{e^{ikr}}{r}\}$. Then the problem is to find the **scattering amplitude** $f(\theta)$, its modulus squared represents the scattering probability in a given direction θ, and it is related to the differential cross section by:

$$D(\theta) = \frac{d\sigma}{d\Omega} = |f(\theta)|^2 \tag{1.22}$$

Capítulo 2

2. FERMILAB

High energy particle accelerators are extrematly neccesary because all theories need their experimental probe, as the standard model and supersimetric models.

2.1 THE TEVATRON AND DØ EXPERIMENT

The Fermi National Accelerator Laboratory (FNAL) is located at west of Chicago in Batavia, Illinois. It was renamed in honor of Enrico Fermi in 1974. Fermilab is the home of the Tevatron accelerator. Two collider experiments, CDF and DØ study the products of interactions of the colliding beams. This graduate work uses information of the Forward Proton Detector FPD located at the DØ interaction point of the Tevatron (Fig2.1).

Fig 2.1 Fermilab

ACCELERATOR CHAIN

The accelerator complex is a chain of particle accelerators at increasing energies and as shown in Figure 2.2. The accelerator complex include:

1. A Cockcroft-Walton Pre-accelerator
2. A LINAC(Linear Accelerator)
3. A Booster
4. The Main Injector
5. An Antiproton Source(Debuncher, Accumulator and Recycler)
6. The Tevatron

Fig 2.2 Accelerator Chain

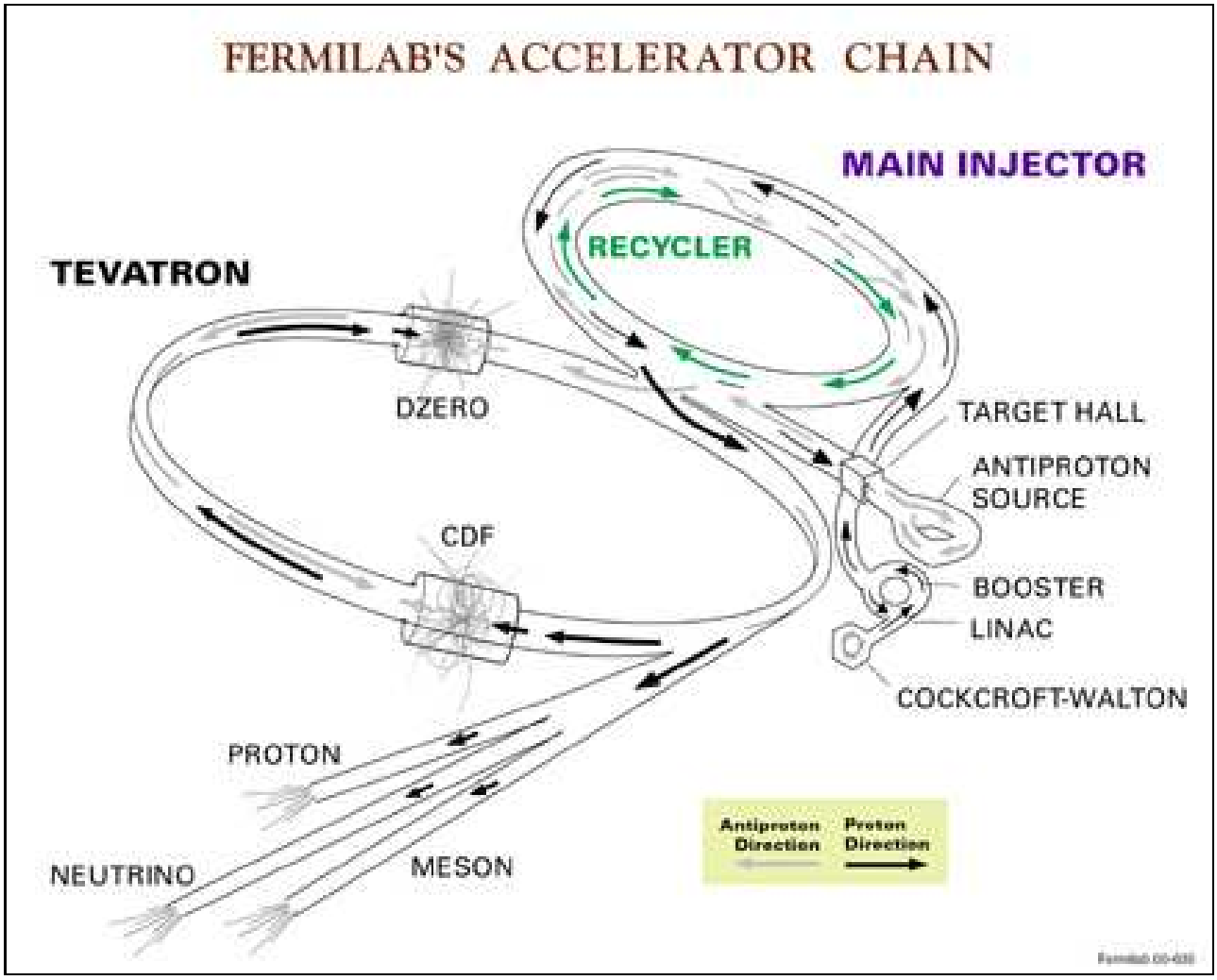

COCKCROFT-WALTON PRE-ACCELERATOR

The first step in the acceleration is to produce the proton beam, this occurs in the Cockcroft-Walton electrostatic pre-accelerator where hydrogen gas is ionized to create H- ions each one is based on two electrons and one proton with a kinetic energy of 18KeV. These ions are accelerated by a positive voltage to 750 keV. This value is around thirty times the energy of an electron beam used in the tube of a tv screen. A transport line of 750 KeV guide the ions from the pre-accelerator to LINAC. A selector guide the beam and determine the

light quantity that is permitted pass to the LINAC[1].

LINAC

From the Proton source the H- ions are led into an approximately 130 meter long linear accelerator (LINAC). In the LINAC, the ions are accelerated to 400 MeV. At the end of the LINAC, the bunches are passed through a carbon foil which strips both electrons from the ions leaving bunches of protons.

BOOSTER

Is a 475 meter circumference fast-cycling synchrotron. This takes the H-ions that come from the LINAC and strips the electrons using a carbon foil. It is located 6 meters underground. With a diameter of 151 meters, the Booster is composed of 18 resonant cavities and 96 magnets to deflect the protons in a circular trajectory and is able to accelerate the beam to energies around of 8 GeV. The protons travel around the Booster proximately 20.000 times. With this energy the proton beam is sent to the main injector.

MAIN INJECTOR

The Main Injector (MI), is a circular accelerator of 3 kilometers of circumference, composed of 18 RF cavities that can accelerate the protons to an energy of 150 GeV. The MI has four principal functions:

A. Accelerate proton bunches from the Booster to 150 GeV
B. Accelerate proton bunches from the Booster to 120 GeV which are then used for simultaneous antiproton production and fixed target/neu rino production
C. Receive antiproton bunches from the Accumulator or the Recycler and increase their energy to 150 GeV in preparation for injection into the Tevatron
D. Inject the proton and anti-proton bunches into the Tevatron.

ANTIPROTON SOURCE

To produce antiprotons, proton bunches accelerated to 120 GeV are extracted from the MI every 1.5 seconds and collided with a nickel target at the Target Station in the Antiproton Source. Protons in the bunches interact with protons in the nickel to produce a proton - antiproton pair. A lithium target acts as a lens to focus the resultant particle bunch into a linear beam that is passed through a pulsed magnet which acts as a mass-charge spectrometer. This is a process, with approximately 20 antiprotons produced for every 1 million protons hitting the target. Because of the messy nature of this collision process, there is a

[1] M. Strang *First observation of dijet events with an antiproton tag at* $\sqrt{s} = 1{,}96TeV$ *using the DØ forward proton detector*, PhD, Thesis, The University of Texas at Arlington, 2005.

large spread in the momentum of the resulting antiprotons. These antiprotons are focused and collected into the Debuncher where large energy fluctuations with a small time spread are transformed into a small energy fluctuations with a large time spread. Before the next bunch from the MI, the cooled antiprotons are passed onto the Accumulator storage ring where they are stored. The antiprotons of the Accumulator that returning from the Tevatron can be inserted into the Recycler for longer term storage before being injected. The Recycler, which shares the same tunnel as the MI, can increase the number of antiprotons produced and available forc ollisions since the production efficiency for antiprotons decreases as the number being stored in the Accumulator increases[1].

TEVATRON

Bunched protons and antiprotons are inserted into the 7 Kilometers circumference Tevatron ring from the MI and accelerated to 980 GeV. The beams are focused and steered around the ring using 216 quadrupolar and 774 dipolar separate superconducting magnets. Once the bunches are accelerated, the two beams are brought to collision at a center-of-mass energy of $\sqrt{s} = 1{,}96$ TeV at two pre-determined points around the ring at which the CDF and D$\emptyset$ detectors are located. The current that pass trough of the magnets is bigger than 4000 amperes, for this reason the magnets remain in a temperature of 4.3 Kelvin, furthermore is necessary to have a cooling station with liquid helium. The magnetic field in each of these magnets is around 4 Teslas. The system of cryogenic cooling is the biggest in the world and is able to produce 1000 liters per hour of liquid helium at 4.2 Kelvin[2].

2.2 D$\emptyset$ EXPERIMENT

GENERALITIES OF THE D$\emptyset$ EXPERIMENT

In the Tevatron accelerator there exists two colllision points and these are surrounded by detectors, the CDF(Colider Detector at Fermilab) and the D$\emptyset$. The principal idea of this graduate work is to focus on the D$\emptyset$ detector and specially in the FPD sub-detector. The D$\emptyset$ detector has proximately 10 meters of lenght and 15 meters of height. The detector consists of four principal parts: Tracking System, Calorimeter, Muon System and Trigger System.

The Tevatron is a big scale accelerator, its radius is approximately of 1 kilometer. The accelerator is divided on six sections called A,B,C,D,E,F. Each section its divided in four subsections called 0,1,2,3. Then due to the place where it is located the D$\emptyset$ detector on the Tevatron receives its name[3].

[2] J. Betancourt *Medicion de la sección eficaz diferencial elástica*, Tesis de Maestría, Universidad de los Andes, 2004.

[3] J. Villamil, *Mediciones de dispersión elástica con el detector FPD en el experimento* $D\emptyset$, Proyecto de grado para optar al titulo de Físico, Universidad de los Andes, 2002.

TRACKING SYSTEM

The measurements nearest of collision point are made with silicon detectors. These detectors give exact information, but for its cost are located the nearest possible to the interaction point to reduce the surface that these detectors has to cover. The information obtained by the silicon detectors can be used to identify quarks bottom, like the produced in the Higgs particle decay. On the outward part of the silicon detectors, the DØ has a tracking system made of scintillating fibers. The Full tracking system is introduced in a powerful magnetic field, then the trajectory of the scattered particles is changed and it is possible to determine the particle's momentum.

CALORIMETER

Surrounding the tracking system a dense absorption system is located to capture particles and to measure their energy. The absorption system is called Calorimeter. The system use metal of uranium covered on liquid argon. The uranium makes that the particles interact and lose energy, the argon detect the interactions and then produces an electrical signal that is possible to measure[1].

MUON SYSTEM

The most outward layer of detectors is able to detect muons. The mouns are unstable particles, but they have enough lifetime to travel trough the whole detector. High energy muons are sign of interesting collisions. Because the Muon System must cover all the detection system is very extensive and it is the first thing that is observed on the DØ assembly.

TRIGGER SYSTEM

The DØ experiment requires three trigger levels to take data. The Proton-Antiproton collisions occur inside the detector with a frequency of 2.5 millions of collisions per second, then it is impossible to store the information of all the produced events. It is neccesary to identify the interesting events and to store them. The trigger system is composed of fast electronics and computers that decide if an event is interesting or not.

REGION OF SMALL ANGLES

This region is useful for the study of diffractive and elastic events. The central DØ detector does not have coverage for small angles, for this reason the forward proton detector was installed. For this graduate work we make use of the FPD.

Fig 2.3 DØ Detector

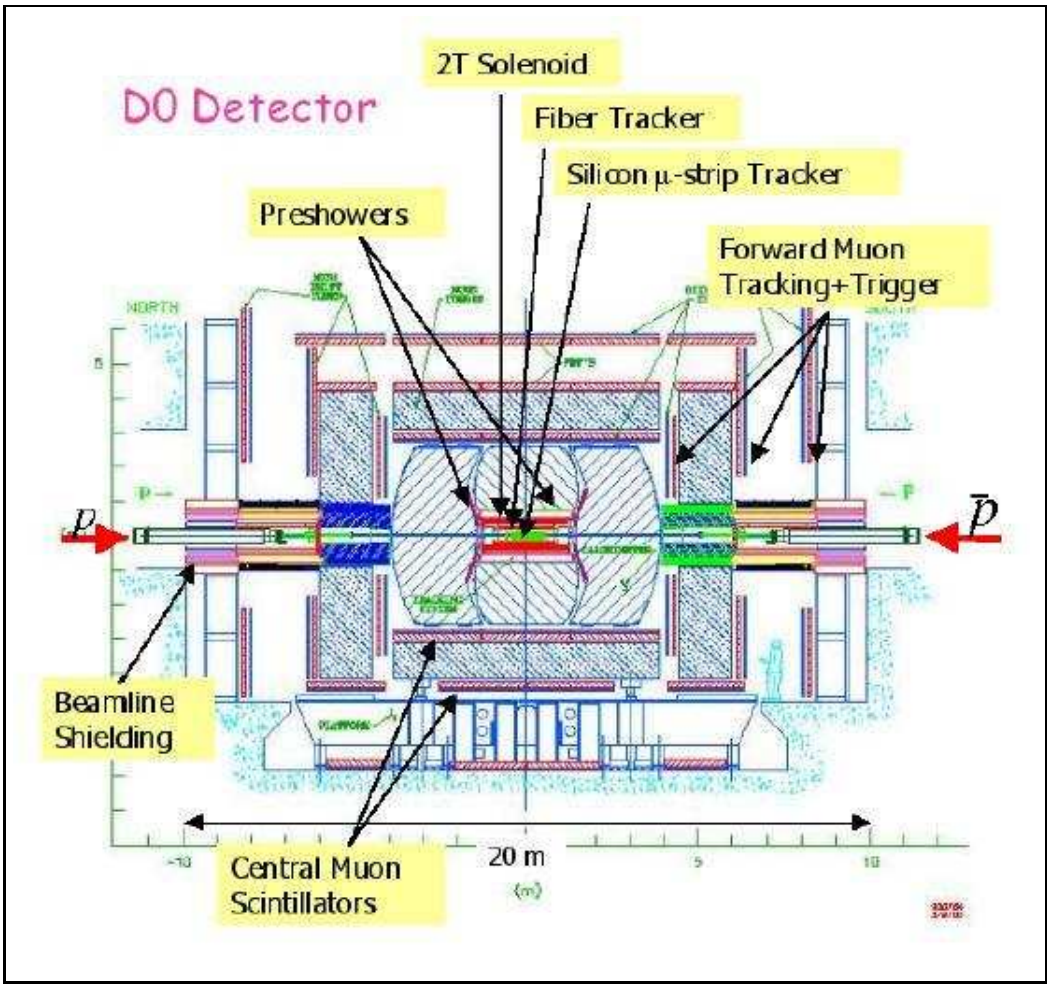

Capítulo 3

3. FORWARD PROTON DETECTOR

Fig 3.1 Forward Proton Detector

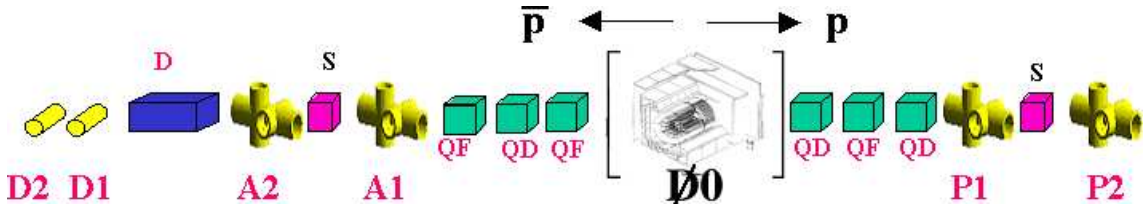

The FPD is a subdetector of the D$\emptyset$ experiment that consists of quadrupolar and dipolar spectrometers that track the scattered protons and antiprotons with low momentum transfer in diffractive collisions. The FPD uses roman pots that contain the detectors, these are located near the beam using motors with a precision of 4.5 μm[1]. All these instruments are driven from the control room. In this graduate work we are going to analyze information of first hand that have been taken on these part of the D$\emptyset$ experiment.

3.1 DIPOLAR AND QUADUPOLAR SPECTROMETERS

The dipolar spectrometers are formed by two roman pot detectors($D1$ and $D2$) located after of the magnet deflection dipoles located 57 and 59 meters from the interaction point in the scattered antiprotons side. The quadrupolar spectrometers are formed by four detectors tagged as **P1**($P1U, P1I, P1D$ and $P1O$), **P2**, **A1**, **A2**. The upper arm coressponds to U and the lower is tagged as D, the inner arm is tagged as I and the outer arm is O[2]. The distances from the interaction point are: 23 meters for A1 and P1, 31 meters for A2 and P2. In table 3.1 shows the names of the spectrometers with their corresponding detectors.

3.2 ROMAN POTS

The Roman Pots are built in stainless steel and contain the detectors, in each run the detectors are moved near the beam and at the end, they are moved out to the original positions. The Roman Pots are located in chambers denominated *Castles*, each Castle of inoxidable steel has an ionic bomb that allows to the Castle to reach the desired vaccum level, Fig 3.2

The FPD consists of 18 Roman Pots that are contained on six Castles, four of them are in the antiproton side ($A1, A2, D1$ and $D2$) after the quadrupole magnets and two of them in the proton side ($P1$ and $P2$) after the quadrupole magnets at each side of interaction

[1] J. Molina, *Estudo do espalhamento elástico em colisões $p\bar{p}$ a $\sqrt{s} = 1{,}96TeV$ com o Detector de Prótons Frontais FPD*, Tese Doutorado, Centro Brasileiro de Pesquisas Físicas, Rio de Janeiro, Septembro de 2003.

[2] The $D\emptyset$ Collaboration, *Proposal for a Forward Proton Detector at $D\emptyset$*, Fermilab-Pub-97-377, 1997.

Fig 3.2 Diagram of a FPD castle

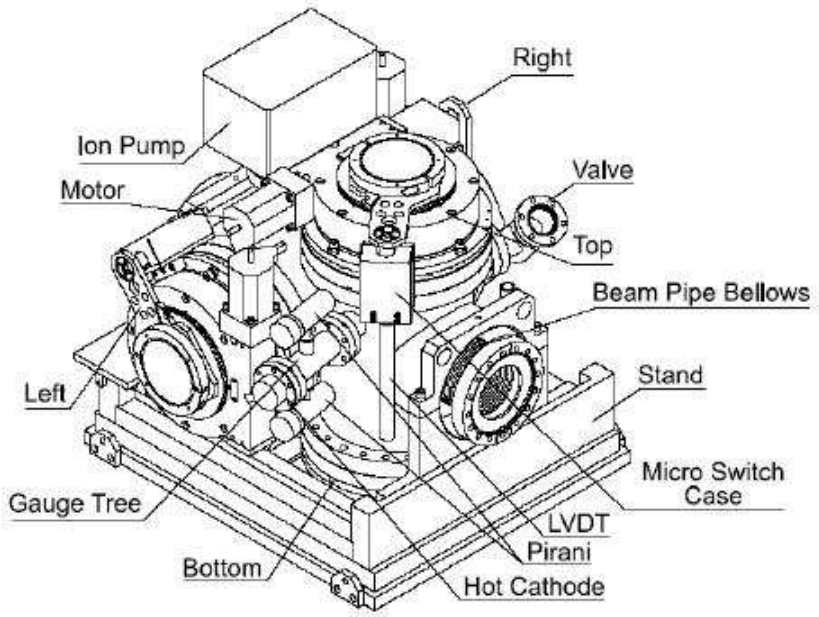

point. The motion of the pots is controlled from the main control room of the experiment with the help of software. There exists a lot of software routines that protect the equipment from accidents.

3.3 SCINTILLATING FIBERS

Each detector consists of six layers which are arranged in three planes (U,X,V). Each plane is made up of a primed and an unprimed layer with the primed layers being offset two-thirds of a fiber width with respect to the unprimed layer. In each detector there is also a trigger scintillator located between the X and V frames with an active area of approximately 2X2 cm^2. The three plastic frames that make up the planes are held together and

Table 3.1.Spectrometers and detectors

Spectometer	Detector 1	Detector 2
PU	P1U	P2U
PD	P1D	P2D
PI	P1I	P2I
PO	P1O	P2O
AU	A1U	A2U
AD	A1D	A2D
AI	A1I	A2I
AO	A1O	A2O
DI	D1I	D2I

Table 3.2 Characteristics of the planes primed and unprimed

Plane	Channels	width(μm)	gap(μm)	offset(μm)	orientation
U	20	780	270	-	45
U‘	20	780	270	270	45
V	20	780	270	-	135
V‘	20	780	270	270	135
X	16	780	270	-	90
X‘	16	780	270	270	90
Total	112	780	270		

aligned trough the use of bolts trough the U and V frames into the X frames. The channels of the U, V planes are oriented at 45 and -45 degrees with respect to the horizontal bottom of the detector.

There are twenty channels in each layer of the U and V planes and sixteen channels in each of the X layers. Thus, there are 112 channels (each with 4 fibers) per detector giving a total of 2016 channels for the full system. On the top of the figure 3.3 it is shown the scheme of the photomultiplier tube and in the bottom it is shown how the four scintillating fibers are arrenged on interface with the anode of the tube.

3.3 Scheme of Scintillating fibers

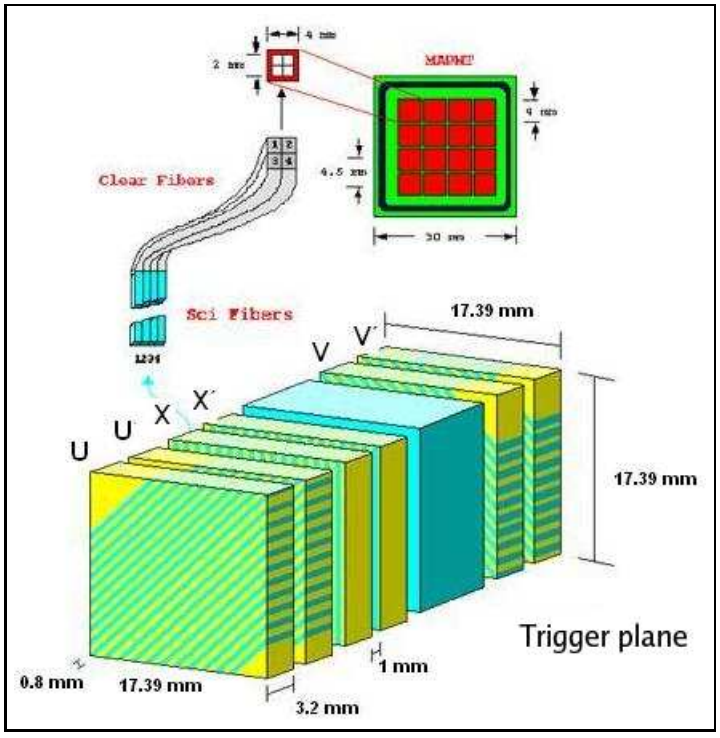

3.4 COORDINATE SYSTEM OF THE FPD

The Forward Proton Detector works with the same coordinate system used in the Tevatron that is based on the reference orbit. It uses a rigth handed system (x, y, z), where z is tangent to the reference orbit, the x coordinate is positive on the outward radial direction while the y coordinate is positive upward . The protons travel in the direction where z increases, finally the orientation of the z and x axis change as the beam is been deflected by the dipolar magnets.[3] For problems like magnets misaligment and deviations on the magnitude of the electric fields, the trajectory of the particles dont coincide with the orbit of reference. In the Tevatron the closed orbits are made intentionally using the dipolar magnets. The separators trough electric fields separate the trajectory of the protons and antiprotons generating separated orbits in all the ring except on the interaction points (D∅, B∅). Each detector that belongs to the FPD has its own coordinate system tagged as (X_d,Y_d), besides each plane on the detector has its own orientation because is rotated or translated as it is shown in the figure 3.4. To each plane it is assigned the respective coordinate system u_d and v_d for the case of the planes U and V, then the relationship between the detector reference system and the plane reference system is:

$$\begin{pmatrix} x_d \\ y_d \end{pmatrix} = \begin{pmatrix} \cos\theta_d & -\sin\theta_d \\ \sin\theta_d & \cos\theta_d \end{pmatrix} \begin{pmatrix} v_d \\ u_d \end{pmatrix} + \begin{pmatrix} 17{,}39/2(mm) \\ -17{,}39/2(mm) \end{pmatrix} \tag{3.1}$$

Where $\theta = 45$ degrees and $17{,}39(mm)$ corresponds to the total detector width.

Fig 3.4.Detector Coordinate System

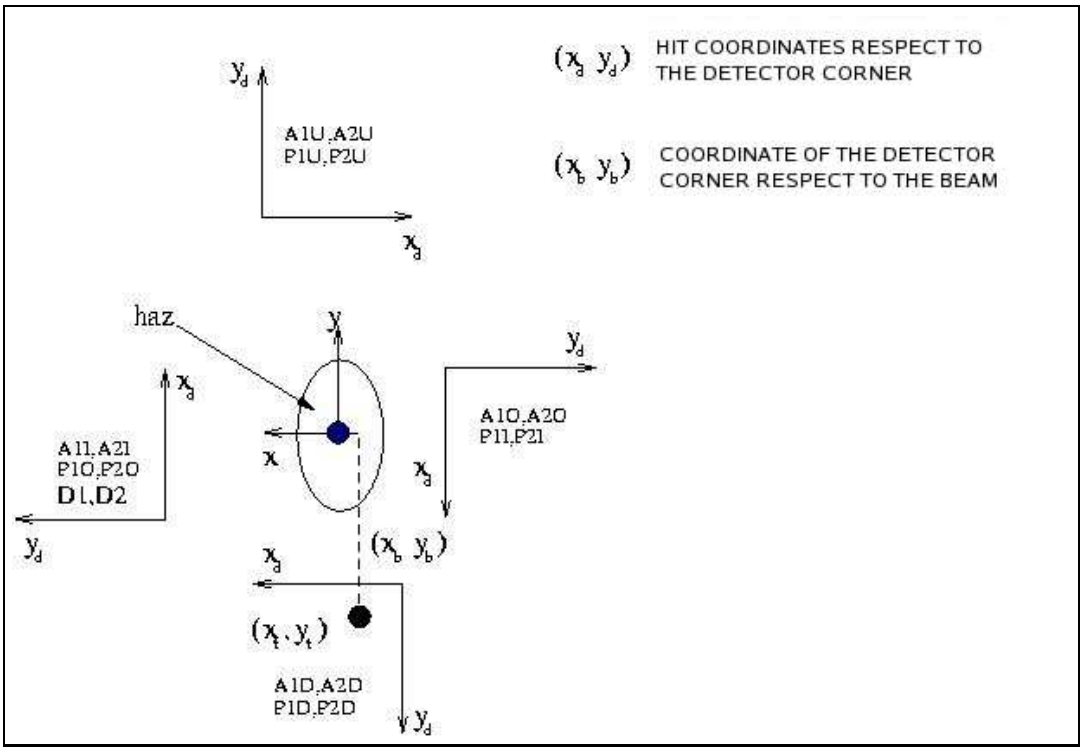

[3] M. Martens , “Coordinate System and Naming Conventions for the FPD Roman Pots”

3.5 BEAM POSITION

Finally we are interested in the coordinates (X_t,Y_t) where the particle hits the detector with respect to the beam as it is shown in figure 3.4. The coordinate system X_d, Y_d moves with respect to the beam position because the motion of the roman pots. Then we must define the positions $X_p = X_d = 0$ and $Y_p = Y_d = 0$ with respect to the reference orbit, furthermore because the beam isn't in the reference orbit (ideal orbit) the coordinates X_b, Y_b are used to define the real position of the beam with respect to the reference orbit. For anyone detector the coordinates are given by:

$$\begin{aligned}
(P1U) -> (x_t, y_t) &= (-x_d, y_d) + (x_p, y_p) - (x_b, y_b) \\
(P1I) -> (x_t, y_t) &= (-y_d, -x_d) + (x_p, y_p) - (x_b, y_b) \\
(P1D) -> (x_t, y_t) &= (x_d, -y_d) + (x_p, y_p) - (x_b, y_b) \\
(P1O) -> (x_t, y_t) &= (y_d, x_d) + (x_p, y_p) - (x_b, y_b) \\
(A1U) -> (x_t, y_t) &= (x_d, y_d) + (x_p, y_p) - (x_b, y_b) \\
(A1I) -> (x_t, y_t) &= (-y_d, x_d) + (x_p, y_p) - (x_b, y_b) \\
(A1D) -> (x_t, y_t) &= (-x_d, -y_d) + (x_p, y_p) - (x_b, y_b) \\
(A1O) -> (x_t, y_t) &= (y_d, -x_d) + (x_p, y_p) - (x_b, y_b)
\end{aligned} \tag{3.2}$$

As we see the coordinates X_d, Y_d are negative sometimes because these are in a opposite direction to the beam coordinates.

3.6 TRIGGER AND DATA ACQUISITION SYSTEM

In a $p\overline{p}$ colliding-beam experiment, only a few events in the millions of collisions per second are selected. As the total collision rate by far exceeds the rate at which events can be recorded (because of dead-time in the electronics) and processed (because of constraints on the cost of storage media and ability to analyze the data), most of the events are discarded. For the events that are recorded, a balance is maintained between different physics processes based on the research priorities of the collaboration. This task of selecting the desired events is accomplished through the use of triggers. A trigger looks at the coarse detector information of one or several subsystems in an event and quickly decides whether to keep or reject it according to a specified criteria. The D$\emptyset$ trigger framework is organized into three main levels (L1, L2 and L3) of increasingly sophisticated event selection and therefore decreasing output rate (the rate is reduced from 1.7 MHz at the beginning down to a rate of 50 Hz for storage to tape). To reduce the rate further, a prescale factor can be applied to triggers. The prescale allows a set fraction of events that pass a trigger decision to propagate through the data acquisition chain. Prescale values may be changed during the course of a store based on instantaneous luminosity. Figure 3.5 shows a schematic diagram of the trigger and data acquisition system[4].

The L1 trigger is a hardware based system using simple algorithms implemented in Field Programmable Gate Arrays (FPGAs) operating on the raw data from a detector. Each individual trigger decision is sent to a so-called Level 1 AND-OR term. All of the data is processed in parallel. Since

[4] M. Strang *First observation of dijet events with an antiproton tag at* $\sqrt{s} = 1{,}96TeV$ *using the D$\emptyset$ forward proton detector*, PhD, Thesis, The University of Texas at Arlington, 2005.

3.5.Trigger and Data Acquisition System

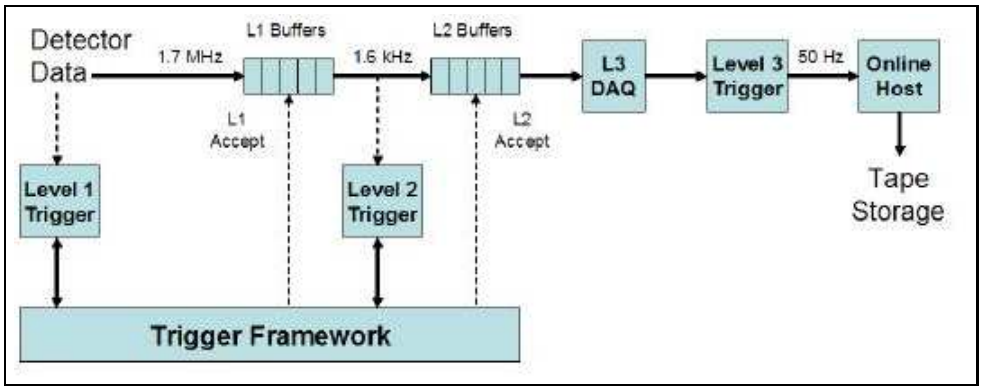

the rate of data acquisition exceeds the processing speed, events are stored in a buffer system[5]. If an event fulfills a trigger criteria a L1 Accept decision is send out (on the order of 3.3 μs) at which point the event is either discarded or passed onto the L2 trigger. At L1, the rate is reduced from 1.7 MHz to about 1.6 kHz. The L2 trigger can be used to apply further selection criteria and improve filtering and in its final stages can also combine the information from different subdetectors[4].
It an event is accepted by level 2, it is passed onto the L3 Data Acquisition System (L3DAQ). The rate is reduced from 1.6 kHz to about 800 Hz by level 2. At the L3 farm, the trigger combines and partially reconstructs the full data for each event that has passed the L1 and L2 decisions. The L3 farm contains software based triggers that run on a farm of Linux PCs. Each event passing L2 is analyzed by a different process which runs an independent instance of the L3 filtering software. Typically events take less than 100 ms to process. The farm nodes receive data fragments through the main switch. A farm node builds a complete event, reconstructs it and performs physics selection. Events that pass the final physics criteria are sent via the network to a collector machine where they are eventually written to tape for offline analysis at the rate of about 50 Hz.

[5]Leo W. R., *Techniques for Nuclear and Particle Physics Experiments*, Springer-Verlag, New York, (1994).

Capítulo 4

4. TRAJECTORIES RECONSTRUCTION

The trajectories reconstruction can be made in two different ways. One is using a program developed by Brasilian investigators which reconstruct the particles trajectory from the interaction point to the detectors. This program has all the information of the Tevatron lattice about the quadrupolar magnets, dipolar magnets, electrostatic separators and other elements near the interaction point. The second form is doing a reconstruction of coordinates using the concept of effective lenghts shown at the end of the chapter. For the analysis of elastic events we will use the second method mentioned for trajectories reconstruction.

4.1 HOW IS THE RECONSTRUCTION DONE?

To reconstruct the particle trajectory we must know the coordinates x_1, y_1 and x_2, y_2 in anyone spectrometer using the information of the hit fibers in each detector, to accomplish this we use a program that reads the number of hit fibers and give as results the coordinates in each detector, with these parameters we can obtain the momentum lost by the particles: $\xi = 1 - x_p = \Delta p/p$ and the four-momentum transfer by the proton $t = (p_{haz} - p)^2$.

PROPAGATION

To identify each one of the elements that compose the Tevatron lattice and the effect that these make over the particles, to each physical element a vector of six elements its assigned that contains the information of the position, deflection, and the lose momentum by the particles in some particular point. The vector is given by:

$$X = (x, y, z, \theta_{xz}, \theta_{yz}, \xi) \tag{4.1}$$

Where x, y and z corresponds to the particle coordinates in some particular point, θ_{xz} and θ_{yz} corresponds to the proyections of the deviations over the X and Y planes of the scattered particles trajectory and ξ corresponds to the fraction of momentum lost. Each time that a particle travels trough an element of the lattice values are assigned to these variables. Then the reconstruction process can be thought as a linear transformation trough the lattice and it is described for the process that will be explained below.[1]

PROPAGATION IN DRIFT SPACES

In the regions where there are not magnets the particles travel free and the trajectory is given by a vector of six elements, and the pass trough the drift spaces is calculated as the product of the position vector on the entry sector(i) of the particle multiplied by the matrix that describes the drift space given as result a vector of six elements on the exit point(f), the equation can be described

[1] J. Barreto and A. Drozdhin *Reconstructing Track Trajectories for the FPD*, $D\emptyset$ Note 3788, 2000.

by:

$$\begin{pmatrix} x_f \\ y_f \\ z_f \\ \theta_{xzf} \\ \theta_{yzf} \\ \xi_f \end{pmatrix} = \begin{pmatrix} 1 & 0 & 0 & d & 0 & 0 \\ 0 & 1 & 0 & 0 & d & 0 \\ 0 & 0 & 1 & 0 & 0 & 0 \\ 0 & 0 & 0 & 1 & 0 & 0 \\ 0 & 0 & 0 & 0 & 1 & 0 \\ 0 & 0 & 0 & 0 & 0 & 1 \end{pmatrix} \begin{pmatrix} x_i \\ y_i \\ z_i \\ \theta_{xzi} \\ \theta_{yzi} \\ \xi_i \end{pmatrix} + \begin{pmatrix} 0 \\ 0 \\ d \\ 0 \\ 0 \\ 0 \end{pmatrix} \tag{4.2}$$

Where d corresponds to the lenght of the drift space.

PROPAGATION THROUGH MAGNETS AND SEPARATORS

Other type of element is the quadrupole magnet which focuses the beam in one direction while defocusing in the other direction. A triplet of quadrupole magnets comprised of focusing (F) and defocusing (D) magnets (F, D, F for example) provides focusing in both directions. The appropriate transport equation is

$$\begin{pmatrix} x_f \\ y_f \\ z_f \\ \theta_{xzf} \\ \theta_{yzf} \\ \xi_f \end{pmatrix} = \begin{pmatrix} T_{11} & 0 & 0 & T_{14} & 0 & 0 \\ 0 & T_{22} & 0 & 0 & T_{25} & 0 \\ 0 & 0 & 1 & 0 & 0 & 0 \\ T_{41} & 0 & 0 & T_{44} & 0 & 0 \\ 0 & T_{52} & 0 & 0 & T_{55} & 0 \\ 0 & 0 & 0 & 0 & 0 & 1 \end{pmatrix} \begin{pmatrix} x_i \\ y_i \\ z_i \\ \theta_{xzi} \\ \theta_{yzi} \\ \xi_i \end{pmatrix} + \begin{pmatrix} b_1 \\ b_2 \\ b_3 \\ b_4 \\ b_5 \\ b_6 \end{pmatrix} \tag{4.3}$$

Where the matrix elements for the focusing magnet are given by:

$$\begin{aligned} T_{11} &= \cos(L\sqrt{k}) \\ T_{14} &= \frac{1}{\sqrt{k}} \operatorname{sen}(L\sqrt{k}) \\ T_{22} &= \cosh(L\sqrt{k}) \\ T_{25} &= \frac{1}{\sqrt{k}} \operatorname{senh}(L\sqrt{k}) \\ T_{41} &= -\sqrt{k} \operatorname{sen}(L\sqrt{k}) \\ T_{44} &= T_{11} \\ T_{52} &= \sqrt{k} \operatorname{senh}(L\sqrt{k}) \\ T_{55} &= T_{22} \end{aligned} \tag{4.4}$$

And for a quadrupole magnet of defocusing in the vertical plane:

$$\begin{aligned} T_{11} &= \cosh(L\sqrt{k}) \\ T_{14} &= \frac{1}{\sqrt{k}}\,\mathrm{senh}(L\sqrt{k}) \\ T_{22} &= \cos(L\sqrt{k}) \\ T_{25} &= \frac{1}{\sqrt{k}}\,\mathrm{sen}(L\sqrt{k}) \\ T_{41} &= \sqrt{k}\,\mathrm{senh}(L\sqrt{k}) \\ T_{44} &= T_{11} \\ T_{52} &= -\sqrt{k}\,\mathrm{sen}(L\sqrt{k}) \\ T_{55} &= T_{22} \end{aligned} \tag{4.5}$$

The quadrupole coefficient k depends on the particle momentum expressed as $(1-\xi)$, the magnet field gradient G and the magnetic rigidity of equilibrium momentum P_{beam}:

$$k = \frac{G}{0{,}33356405 P_{beam}(1-\xi)} \tag{4.6}$$

where the the beam momentum is 980 GeV and the field gradient is accessed through a database provided by the Accelerator Division based on the current in the magnet for a particular store. After the quadrupoles, the particle passes through three electrostatic separators[2] which provide horizontal (H) and vertical (V) electric fields. The particle passes through the separators in the order V, H, V. These fields control the separation between the p and $\bar{p}$ beams which travel around each other in a helical orbit around the Tevatron ring until they are focused at an interaction region. A separator can be modeled either as a dipole magnet with a magnetic field equivalent to the electric field or by a Mike Martens model where the separator is approximated by two drift spaces with an appropriate kick in between the drifts whose strength depends on the maximum electric field between the separator plates. In general we can thought in a linear transformation and for the case between two detectors, the equation which defines the slope is given by:

$$\begin{aligned} x_1' &= \frac{(x_2 - x_1 - X)}{L_{Total}} \\ y_1' &= \frac{(y_2 - y_1 - Y)}{L_{Total}} \end{aligned} \tag{4.7}$$

Where X is a constant which depends of the horizontal space between the separators and the change in the angle, x_1, y_1 and x_2, y_2 corresponds to the coordinates in the detectors P1D and P2D respectively and L_{Total} is the total lenght between the detectors treated.

In this way the trajectory is reconstructed from the interaction point(IP) to the detectors, the reconstruction process from the interaction point IP to the detector P2 in the proton side is given by:

$$\begin{aligned} X_{p1} &= L_{P_{H1}-P1V} L_{Q_2-P_{1H}} Q_2 L_{Q_3-Q_2} Q_3 L_{Q_4-Q_3} Q_4 L_{IP-Q_4} X_{IP} \\ X_{p2} &= L_{P_{H2}-P2V} L_{S_3-P_{2H}} S_3 L_{S_2-S_3} S_2 L_{S_1-S_2} S_1 L_{P_{1V}-S_1} X_{P1} \end{aligned} \tag{4.8}$$

The parameter that defines X_{IP} is a vector of six components at the interaction point, X_{p1} corresponds to the vector in the detector P1D, X_{p2} corresponds to the vector in the detector P2D, $L_{P_{H1}-P1V}$ is the matrix associated to the drift space between the detctor P1O and the detector P1D, Q_i is the matrix that contains the information of the quadrupolar magnet and S_i is the matrix associated to the separator.

4.2 TRAJECTORIES RECONSTRUCTION

To determine the parameters ξ and $|t|$ in IP the first step consists in converting the information of the hit fibers in coordinates x_1, y_1 and x_2, y_2 on the detectors as described as follows.

COORDINATES RECONSTRUCTION ON THE DETECTORS

The information of the hit fibers is converted to coordinates $x_{d1}, y_{d1}, x_{d2}, y_{d2}$ on the detectors P1D and P2D respectively in the protons case, starting from the number of hit fiber by plane. For this reason a routine is implemented that reconstructs the coordinates using the equation for each fiber. The x coordinate is obtained from the X and X' planes with:

$$X_d(mm) = S_P + (2S_N - 1)H_{WF} + (S_N - 1)Offset \tag{4.9}$$

Indicating S_N as the number of fiber segment in the X and X' planes which is generated by the intersection between two fibers or simply it is given by the width of the fiber as it is indicated on figure 4.1. A segment corresponds to the width of the intersection of the fibers that can result from the intersection of two or three planes, for example a x segment is the fiber segment that results from the intersection of the planes x and x', in a similar way we proceed to construct the u and v segments[2].

Fig 4.1.Segment Width

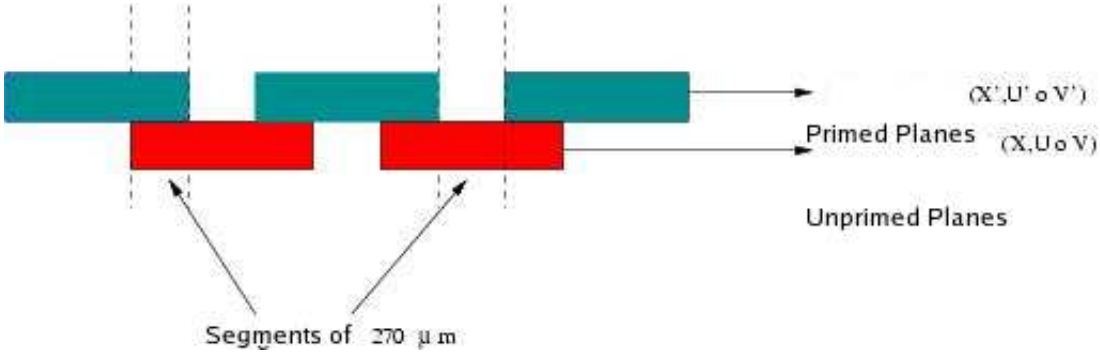

S_P represents the displacement of the primed plane from the border of the detector, H_{WF} corresponds to half of the width of each fiber and the $Offset$ is the separation between each fiber plane. If the particle goes trough the two planes S_N corresponds to the number of segments that

[2] *J. Betancourt* Medicion de la sección eficaz diferencial elástica*, Tesis de Maestría, Universidad de los Andes, 2004.*

are generated by these intersections. For the case of the planes V and V' the assignment is made in similar way. From the values in the fibers in the V plane the intercept is obtained by a linear equation given by 4.10, the coordinate $y(mm)$ that results from the intersection of the planes xv is given by $y_{vx} = -tan(\theta)x_d + bv$ where $\theta = 135^0$:

$$b_v(mm) = S_P + D_C + (2S_N - 1)H_{WF}\sqrt{2} + (S_N - 1)Offset\sqrt{2} \tag{4.10}$$

In a similar way that the last case D_C represents the distance from the corner of the detector to where the first fiber begins,the equation of the intercept that results of the intersection of V and V' planes is based in a number that determines the value of the segment that is obtained trough this intersection. For the U planes the equation is[3]:

$$b_u(mm) = W_D - D_C - S_P - (2S_N - 1)H_{WF}\sqrt{2} + (S_N - 1)Offset\sqrt{2} \tag{4.11}$$

Where W_D corresponds to the real width of the detector. The y coordinate of the detector is obtained from $y_{ux} = -tan(\theta)x_d + bu$, where $\theta = 45^0$, due to the fact that the plane is rotated with respect to the X plane. In the case of intersection between the U and V planes the coordinates are obtained from:

$$\begin{aligned} x_{uv}(mm) &= (b_v + b_u)/2 \\ y_{uv}(mm) &= (b_v - b_u)/2 \end{aligned} \tag{4.12}$$

With the previous equations we can obtain the coordinates x_{uv}, y_{uv}, x_{ux}, y_{ux} and x_{vx}, y_{vx} and then calculate $x_d = (x_{uv} + x_{ux})/2$. x_d is defined as the average beacuse x_{ux} and x_{vx} are obtained from the same equations that result from the X plane, in this way $x_{ux} = x_{vx}$, while $y_d = (y_{uv}+y_{ux}+y_{vx})/3$ result is different for the three intersections as it is shown in figure 4.2. For this reason the geometric center of the intersections is chosen. A new file that contains the run number, event number, and the respective coordinates by detector is obtained[3].

Fig 4.2.Determination of the particle hit coordinate in the detector system

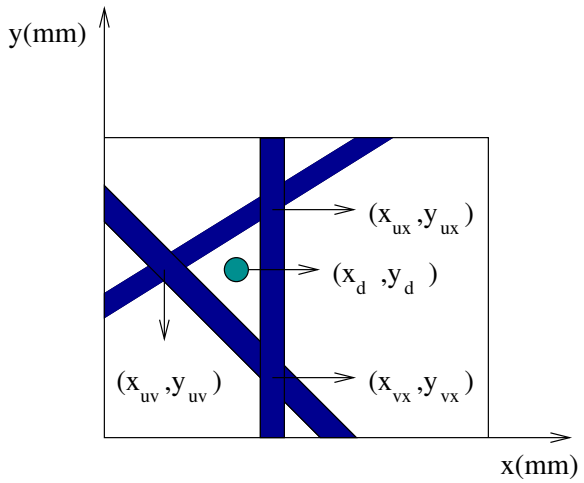

IP COORDINATES

The following step consists in obtaining the values x', y' in P1D using the coordinates in the P1D, P2D detectors and then proceed to obtain the coordinates x_0, y_0 at the interaction point using a reconstruction that is based on a linear transformation described by:

$$X_{IP} = (L_{P_{H1}-P_{1V}} L_{Q_2-P_{1H}} Q_2 L_{Q_3-Q_2} Q_3 L_{Q_4-Q_3} Q_4 L_{IP-Q_4} X_{P1})^{-1} \tag{4.13}$$

With these values we can obtain ξ and t using an iteration process that is described in the next section for all detectors.

BEAM WIDTH AND EFFECTIVE DISTANCES

The position and angle of the particle in some place of the accelerator with respect to the position and the angle of the particle at the interaction point can be obtained using the transport matrix M_{01}[3]:

$$\begin{pmatrix} y_1 \\ y_1' \end{pmatrix} = M_{01} * \begin{pmatrix} y_0 \\ y_0' \end{pmatrix} \tag{4.14}$$

With M_{01} given by:

$$M_{01} = \begin{bmatrix} (\beta_1/\beta_0)^{1/2}(cos\Delta\mu + \alpha_0 sin\Delta\mu) & (\beta_0\beta_1)^{1/2} sin\Delta\mu \\ -(1+\alpha_0\alpha_1 sin\Delta\mu + \alpha_0\alpha_1 cos\Delta\mu)/(\beta_0\beta_1) & (\beta_0/\beta_1)^{1/2}(cos\Delta\mu - \alpha_1 sin\Delta\mu) \end{bmatrix} \tag{4.15}$$

Where $\Delta\mu = \mu_1 - \mu_0$ is the phase difference between z_0 (position in $D\emptyset$) and z_1(position in the detector). M_{01} is a 4 x 4 matrix if x and x' are included. The connection between x and y is neglected. From the equation 4.15 we can write:

$$\begin{aligned} y_1 &= m_{01} * y_0 + L_{yeff01} * \theta_y \\ m_{01} &= (\beta_1/\beta_0)^{1/2}(cos\Delta\mu + \alpha_0 sin\Delta\mu) \\ L_{yeff01} &= (\beta_0\beta_1)^{1/2} sin\Delta\mu \end{aligned} \tag{4.16}$$

Where L_{yeff01} is the effective distance in y between the points z_0 and z_1, θ_y is the scattering angle of the particle projected on the vertical plane, y_0 is the offset of the beam in the y direction at the interaction point[3].

The beam width in each detector depends of the emittance (ε_y), the amplitude function β_y and the particle momentum p:

$$\sigma_x^2 = -\frac{\varepsilon_x \beta_x}{2\pi p ln(1-f)} \tag{4.17}$$

A similar equation is used to determine σ_y. The minimum values of $|t|$ can be obtained as:

$$\begin{aligned} t_{minx} &= (\frac{p^2 x^2}{Leff_x^2}) \\ t_{miny} &= (\frac{p^2 y^2}{Leff_y^2}) \end{aligned} \tag{4.18}$$

[3] J. Villamil, *Mediciones de dispersión elástica con el detector FPD en el experimento* $D\emptyset$, Proyecto de grado para optar al titulo de Físico, Universidad de los Andes, 2002.

4.4 SCATTERING ANGLE

The scattering angle is given in terms of its projections over the vertical and horizontal planes according to equation 4.19

$$\theta^2 = \theta_x^2 + \theta_y^2. \tag{4.19}$$

Now considering the scattering in the horizontal plane, the angle can be expressed in terms of the X displacement of the particle registered by the detector, the displacements of the interaction (collision) x_0 and z_0 in the directions x and z respect to the center of the interaction region, the initial angle α_x of the particle that collide with respect to the original orbit, and the transport matrix elements L_x and m_x between the center of the interaction region and detector. The total expression is given by equation 4.20[4] .

Fig 4.3.Trajectory of a scattered particle

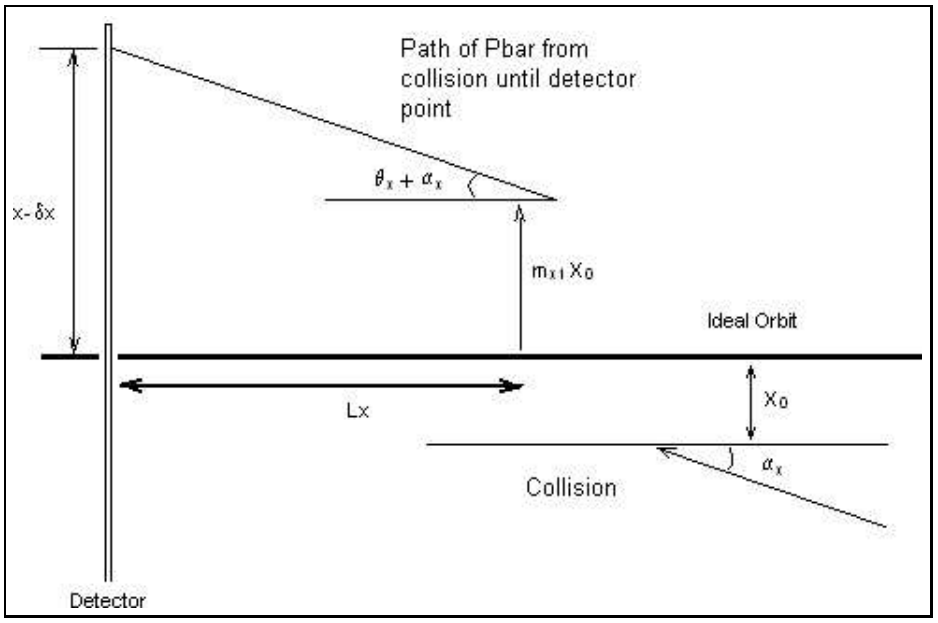

$$\theta_x = \frac{(x - \delta x) - m_x x_0 - \alpha_x L_x}{L_x + m_x z_o}. \tag{4.20}$$

δx corresponds to the difference between the real particle position in the detector and the registered one due to its resolution. Writing the denominator in equation 4.20 as a power series of $\frac{m_x z_0}{L_x}$ one obtains:

$$\theta_x = \frac{(x - \delta x) - m_x x_0 - \alpha_x L_x}{L_x}\left[1 - \frac{m_x z_o}{L_x} + O\left\{\left(\frac{m_x z_o}{L_x}\right)^2\right\}\right]. \tag{4.21}$$

Then the second order terms are negligible and we can write:

$$\theta_x = \frac{(x-\delta x) - m_x x_0 - \alpha_x L_x - \frac{m_x z_o}{L_x}}{L_x} = \frac{x - X_o}{L_x}. \tag{4.22}$$

where,

$$X_o = \delta x + m_x x_o + \alpha_x L_x + \frac{m_x x z_o}{L_x}. \tag{4.23}$$

In a similar way

$$\theta_y = \frac{y - Y_o}{L_y}. \tag{4.24}$$

where

$$Y_o = \delta y + m_y y_o + \alpha_y L_y + \frac{m_y y z_o}{L_y}. \tag{4.25}$$

4.5 BEAM PARAMETERS

In table 4.1 is indicated a list of the beam parameters for the detectors of the FPD with normal run conditions. In this work we use high β conditions.
Table 4.1.Beam parameters for normal run conditions

$\beta_x(m)$	α_x	$\mu_x(2\pi)$	$\beta_y(m)$	α_y	$\mu_y(2\pi)$	pot
154.878	-7.030	6.812	12.789	-1.196	6.733	D2I
188.241	-7.764	6.815	19.150	-1.625	6.756	D1I
736.710	-15.363	6.825	203.160	-6.150	6.818	A2U
736.710	-15.363	6.825	203.160	-6.150	6.818	A2D
741.388	-15.412	6.825	205.035	-6.179	6.818	A2I
741.388	-15.412	6.825	205.035	-6.179	6.818	A2O
1055.183	-18.398	6.826	336.198	-7.953	6.823	A1U
1055.183	-18.398	6.826	336.198	-7.953	6.823	A1D
1049.598	-18.349	6.826	333.785	-7.924	6.823	A1I
1049.598	-18.349	6.826	333.785	-7.924	6.823	A1O
328.930	7.764	7.324	1078.038	18.778	7.321	P1U
328.930	7.764	7.324	1078.038	18.778	7.321	P1D
326.574	7.735	7.325	1072.337	18.728	7.321	P1I
326.574	7.735	7.325	1072.337	18.728	7.321	P1O
199.032	6.006	7.330	752.948	15.684	7.323	P2U
199.032	6.006	7.330	752.948	15.684	7.323	P2D
200.862	6.035	7.330	757.724	15.734	7.323	P2I
200.862	6.035	7.330	757.724	15.734	7.323	P2O

For normal run operations that correspond to the way in which the Tevatron worked for the analyzed data in this graduate work, is assumed a vertical and horizontal emittance of:

$$\varepsilon_x = \varepsilon_y = 20\pi mm - mrad \tag{4.26}$$

Using the equations 4.16, 4.17, and 4.20 the effective lenghts, the beam width and the minimum values of $|t|$ can be determined if the detectors were located to 8σ to the beam. These values are showed in the table 4.2.

Table 4.2.Effective lenghts and beam width for normal run conditions

$L_X(m)$	$L_Y(m)$	$m01_x$	$m01_y$	$\sigma_x(mm)$	$\sigma_y(mm)$	pot
11.086	4.931	-3.217	-5.505	0.271	0.160	D2I
11.658	5.338	-3.179	-5.346	0.282	0.161	D1I
17.642	9.601	-2.773	-1.577	0.410	0.213	A2U
17.642	9.601	-2.773	-1.577	0.410	0.213	A2D
17.678	9.625	-2.779	-1.580	0.410	0.214	A2I
17.678	9.625	-2.779	-1.580	0.410	0.214	A2O
20.010	11.294	-2.591	0.096	0.462	0.249	A1U
20.010	11.294	-2.591	0.096	0.462	0.249	A1D
19.973	11.265	-2.586	0.096	0.461	0.249	A1I
19.973	11.265	-2.586	0.096	0.461	0.249	A1O
11.297	20.014	0.398	0.010	0.263	0.441	P1U
11.297	20.014	0.398	0.010	0.263	0.441	P1D
11.266	19.976	0.397	0.010	0.262	0.441	P1I
11.266	19.976	0.397	0.010	0.262	0.441	P1O
9.594	17.646	-0.493	-0.253	0.221	0.389	P2U
9.594	17.646	-0.493	-0.253	0.221	0.389	P2D
9.620	17.684	-0.457	-0.254	0.221	0.390	P2I
9.620	17.684	-0.457	-0.254	0.221	0.390	P2O

Capítulo 5

5. METHODOLOGY OF THE EFFICIENCY ANALYSIS

In this chapter we treat one important correction that is required for the data analysis: EFFICIENCY OF THE FIBERS. In our work we analyze the efficiency of individual fibers of the FPD. Also we compare our results with other similar studies made in other research institutions. Finally it is presented in a graph sumarizing the efficiency results from some detectors.

5.1 EFFICIENCY OF THE FIBER CHANNELS

All the information necessary for any analysis of the FPD is obtained from the scintillating fibers of each detector. With this information the hit coordinates are determined in the detectors, and then the information is ready to be analyzed. Then the importance lies on how much efficient these fibers are, if these are identifying correctly the particles that go throug them. It is expected that the efficiency values decrease with time due to radiation damage. The number of total fibers analyzed is 2016. For this purpose we have modified for our needs a routine of $C/C++$ and ROOT that was developed recently in FERMILAB by Santiago Gonzales, Duncan Brown and Carlos Avila. It is important to mention that all these routines are modified with the pass of the time because the acquisition systems are changing to obtain better results[1].

Fig 5.1.UVX intersections

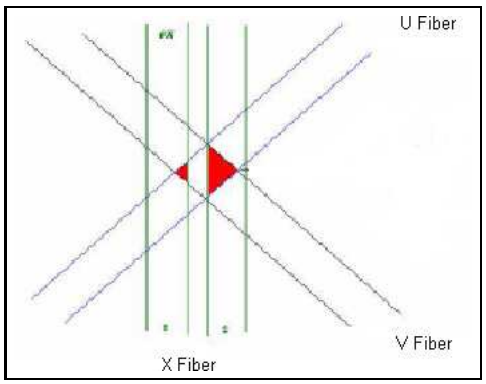

METHODOLOGY

The method consists in cheeking how often a channel is ON when it should have gone ON. "ON" means the channel passed the pedestal and discriminator cuts. In order to do this for finding the efficiency of a particular fiber of a certain plane the software has to check fibers of other planes that intersect within the fiber in consideration to ensure that a particle did go trough it. Four other channels that intersect inside the fiber in consideration are taken into account to calculate the

[1] S. Gonzáles *Prueba de modelos difractivos en el Tevatron*, Tesis de Maestría, Universidad de los Andes, 2005.

efficiency. If those four fibers are $''ON''$ the investigated fiber should also be $''ON''$, if we are for example looking at the efficiency of a X fiber the software will look at other fibers of planes U, U', V, V', forming an overlap completely within the X channel.

There exist two types of analysis due to kind of overlap SMALL and BIG INTERSECTION. For big intersection we look the state of the channels U and V that have an overlap with the X channel If both channels are ON, independently if X is stored we increase the entry in a variable for example N_{uv}. After that is verified if additionally the analyzed fiber is ON, then this result is stored in the N_{uvx} variable. Finally care divide the results to obtain in this way the efficiency of the X fiber. In the same way we find the efficiencies for the other channels[1]:

$$\begin{aligned} e_U &= \frac{N_{UVX}}{N_{VX}} \qquad e_{U'} = \frac{N_{U'V'X'}}{N_{V'X'}} \\ e_V &= \frac{N_{UVX}}{N_{UX}} \qquad e_{V'} = \frac{N_{U'V'X'}}{N_{U'X'}} \\ e_X &= \frac{N_{UVX}}{N_{UV}} \qquad e_{X'} = \frac{N_{U'V'X'}}{N_{U'V'}} \end{aligned} \tag{5.1}$$

In figure 5.1 one can observe intersections or overlaps between three fibers of different planes. For example if we are analyzing the efficiency of the fiber $X-1$, we must look at the number of times that the fibers U and V were ON, and also the number of times that the fiber $X-1$ was ON. In the same way for the fiber $X-2$ taking into account additional overlaps of the fibers U, V. This method, nevertheless, presents some problems because the intersections are big. These problems are because the intersection isn't completely behind of the fibers U, V. Then there are some problems like the overlap of a same intersection UV with two diferent fibers $X-1$ and $X-2$, as it is shown in figure 5.1. In this case, if, for example, the $X-1$ fiber was ON but $X-2$ was OFF, when we evaluate the efficiency of the $X-2$ channel we are expecting that the fiber under consideration should be ON because U and V were ON, when in reality U and V were ON because the particle went trough the $X-1$ fiber. Then for this reason we can obtain wrong efficiency values.

Fig 5.2.$UU'VV'$ X intersections

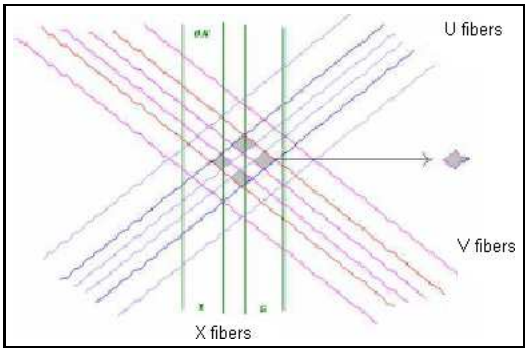

Then to resolve this problem we need to use a more sophisticated process called SMALL INTERSECTION based on smaller intersections. Now we take into account four fibers of different planes

with the goal of restricting the area covered by the intersection of those fibers. For example to measure the efficiency of a X fiber, we look if the fibers U, U', V and V', which form an intersection completely inside the X fiber are ON. In figure 5.2 we can observe that there exist some intersections $UU^{'}$ that are found inside the channel investigated, this ensures that the particle had to go trough the fiber X. In this way, the efficiencies of the fibers only are calculated when the overlap are behind of them, and the equations to calculate efficiencies now are given by:

$$e_U = \frac{N_{UVV'XX'}}{N_{VV'XX'}} \qquad e_{U'} = \frac{N_{U'VV'XX'}}{N_{VV'XX'}} \tag{5.2}$$

$$e_V = \frac{N_{UU'VXX'}}{N_{UU'XX'}} \qquad e_{V'} = \frac{N_{UU'V'XX'}}{N_{UU'XX'}}$$

$$e_X = \frac{N_{UU'VV'X}}{N_{UU'VV'}} \qquad e_{X'} = \frac{N_{UU'VV'X'}}{N_{UU'VV'}}$$

We must take into account other additional effects. One of them consists in that the fibers can be ON due to the activity of other intersections created by other fibers. In figure 5.3a we can observe this effect, where the fibers V, V', U and U' can go ON by particles that go trough other regions of the same fiber. Then when studying the efficiency of the X fiber as it is shown in figure5.3, we expect that the fiber is ON because the fibers U, U' and V, V' go through the analyzed fiber. In reality the fibers V and V' could have gone ON by the passing of a particle in other place (different for the fiber which we want to investigate) confirmed by other fiber U or U'. The fibers V and V' can go ON by particle going through other place as a drift space between fibers. Other example of similar problems is shown in figure 5.3b. Then we have two pairs of fibers UU' and two pairs of fibers VV' that intersects in fourth possible places indicating fourth possible hits. Then it is not possible to know how many and which fibers were ON with the help of the information of the fourth fibers ON mentioned above, and therefore we can't calculate the efficiency value of the X fiber and the efficiency value for other fibers[1].

Fig 5.3a) Hits in other fibers b) Several hits on the investigated fiber

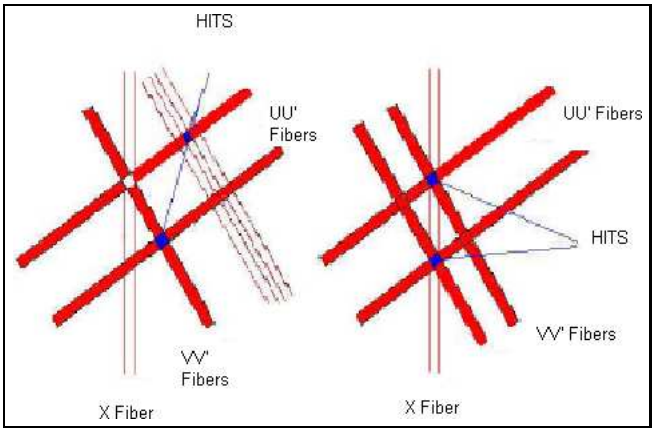

To avoid all the problems mentioned above, only events with few hit fibers are allowed. Specifically it is required that a maximum of 8 fibers be ON by detector. Ideally will be convenient to allow until 5 fibers, 4 that confirm the passing of the particle and the other will be the investigated fiber. This

reduces significantly the statistics, for this reason we use the bigger intersection. With the above considerations we could affirm that the method is complete and effective to calculate efficiency values. An example of the pattern of intersections is shown in figure 5.4. The procedure, newertheless has some disadvantages. One of them is the low statistics due to the few intersections completely within the fibers and also the requirement of several fibers on. The second disadvantage comes from the fact that we have been assuming an ideal geometry and perfect alignment of the detector. In the practice when detectors are assembled, the alignment of them is modified creating offsets between planes that affects the ideal form of the intersection between the fibers.

Fig 5.4.Intersection pattern example of an FPD detector. $UU'VV'$ intersections inside fiber X

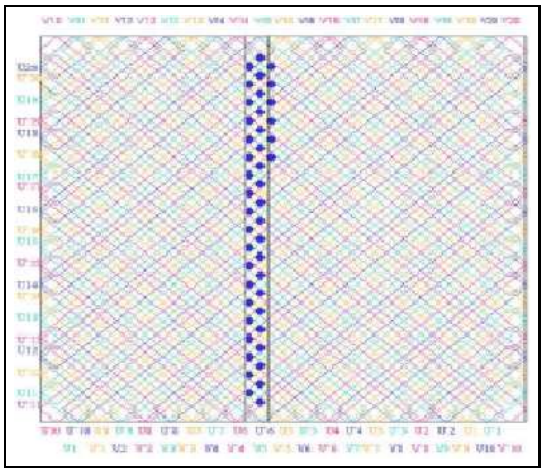

Capítulo 6

6. EFFICIENCY ANALYSIS

In this chapter we analyze all the results obtained in the first part of this work. Also it is shown and explained step by step how the data analysis is performed beggining with the download of the information that is going to be used, following with the data analysis and its correct interpretation and finally some conclusions of the results are given.

6.1 DATA SAMPLE

For the analysis made in this work we use data that were taken in Tevatron store 4647 on the dates of february 17 and 18 of 2006. The runs analyzed are from 215417 to 215449. Special Tevatron conditions were needed for this store in order to locate the FPD Roman Pots as close as possible to the beam center. Electrostatic separators were turned off for this store and scrapping in vertical and horizontal planes was performed to reduce emmitance of the beams. In this first part of the analysis all runs are used with all the events contained in them, because a high statistics is needed to obtain results that can give valuable information about the behavior of the efficiency in the scintillating fibers for all FPD detectors.

Table 6.1 FPD Runs that were selected for this work

ANALYZED RUNS			
RUNS	EVENTS	RUNS	EVENTS
215417	740705	215434	787005
215418	508464	215436	1359433
215421	827303	215440	1012787
215424	1600633	215443	1114845
215425	1220636	215445	789949
215427	8503	215446	14416
215429	4147836	215447	1769842
215430	435472	215448	1591610
215431	6379	215449	1530883
215433	140072		
TOTAL			19606773

To obtain all these Runs, it was neccesary to use a Uniandes computer called dzero1.uniandes.edu.co. In this computer all Runs were stored, and then the work was to download this information that approximattely had a space of 20 Gigabytes. Due to the low speed of the internal network this process took several days.

6.2 SOFTWARE TO CALCULATE THE FIBER EFFICIENCIES

After the information was ready to be used, a program was needed to read out, unpack and make the desired effciency calculation. The software was developed in the master degree thesis of Santiago Gonzales with the help of Duncan Brown and Carlos Avila. Then the first step of our investigation was to understand the program called FIBEF.C because it was necessary to make modifications to test the program with the information that we mentioned above. The program FIBEF.C had problems with the read out of some input files and for this reason the software calculated initially wrong efficiency values. Then the solution was read out in a different way the input files.It is important to mention that the time process of the program was approximately 24 hours for each test. Taking into account that a great quantity of tests were performed with different input conditions that were made in a routine called FIBEF.H to observe, deduce and calculate the best efficiency values taking care of not modifying the methodology to calculate the efficiencies for each fiber.

PEDESTAL AND DISCRIMINATOR CUTS

Inside the program FIBEF.C there exist two routines used to guarantee that a particle has gone through the fibers of interest. The first routine make a pedestla cut. This cut is made to reject electronic noise that can produce fake fibers on. To obtain the proper thresholds to be applied a run with no beam has to be taken in order to measure the electronic noise in each fiber channel. The pedestal values are saved in a PEDESTAL FILE with the format of the mean value and sigma (σ) for each fiber that is need by the program. The cut generally used is the mean value + 4σ this value must be subtracted to the value recorded for the charge of the specific fiber. The charge on each fiber is digitized by using an analog to digital converter (ADC). What we store is not charge but instead ADC counts. If after this subtraction the fiber contain ADC counts then is considered a FIBER ON:

$$ADC_{fiber} \geq PedestalMean_{fiber} + 4 * Pedestal\sigma_{fiber} \rightarrow FIBER \quad ON \tag{6.1}$$

Fig 6.2.Pictures of a COOKIE

0	1	2	3
4	5	6	7
8	9	10	11
12	13	14	15

There is a second cut after pedestal cut, this second cut is the discriminator cut. The discriminator cut is made to counteract other electronic effects due to the configuration of how are arranged the

fibers Fig 6.2[1] between them (cookies) there could be cross talk in the neigbboring channels of a cookie.

$$ADC_{fiber} \geq PedestalMean_{fiber} + 4 * Pedestal\sigma_{fiber} + Discriminator_{MAPMT} \tag{6.2}$$

6.3 EFFICIENCY RESULTS

After pedestal and discriminator cuts are applied we start the efficiency analysis. The program that determine the efficiencies provides a file.txt which has the following information:
1. Detector
2. Plane: Plane in which is the fiber analyzed
3. Num1: Stored value for example in $e_U \rightarrow Num1 = N_{VV'XX'}$
4. Num2: Stored value for example in $e_U \rightarrow Num2 = N_{UVV'XX'}$
5. Efficiency: Then is made the division:

$$\varepsilon_u = \frac{N_{UVV'XX'}}{N_{VV'XX'}} \tag{6.3}$$

This is equation 5.2 that determines the efficiency of a fiber in the U plane.

For the calculation of Num1 and Num2 the program uses the methodology explained in chapter five.
Then having the output file we can obtain and analyze the following results:
A. Zero efficiency values
B. High and low efficiency values

The zero efficiency values can be produced by two different ways:
1. In the set of equations 5.2 if the numerator is zero and the denominator is different from zero this means that the fiber analyzed have a zero efficency value, this can be guaranteed only if the denominator has a high statistics.
2. If the numerator and denominator are zero. This means that the program could have had problems with the efficiency calculation for the last fibers in each plane and their intersections with neighborhood fibers.

In the table shown below we have registered the quantity of zero efficiency values found in the output efficiency file and are underlined with red the detectors that are most affected. Two tests were made, TEST 1 was done with the set of runs 2045311 to 2049621 (26 runs taken on february 11), TEST 2 was done with all runs analyzed in this work: 215417-215449. Furthermore a comparison is make with results obtained by Brasilian researchers with the same program and some different input conditions. Table 6.2
It is clear that both analysis show similar results about the detectors most affected due to the zero efficiency values. In the next chapter we will analyze elastic events and the detectors performance. We obtain results for efficiencies of all detectors. To show all efficiency results 108 histograms are needed, therefore only we show in this work a few representative histograms.Fig 6.3, 6.4, 6.5, 6.6.

[1] M. Strang *First observation of dijet events with an antiproton tag at* $\sqrt{s} = 1{,}96TeV$ *using the DØ forward proton detector*, PhD, Thesis, The University of Texas at Arlington, 2005.

Table 6.2 Zero Efficiency Values

DET	BRASIL	TEST 1	TEST 2	BRASIL %	TEST 1 %	TEST 2 %
A1U	5	6	4	0.99	0.90	0.91
A1D	14	7	6	2.76	1.06	1.37
A1I	10	16	5	1.97	2.42	1.14
A1O	13	13	7	2.56	1.97	1.59
A2U	**92**	**100**	**87**	**18.14**	**15.15**	**19.82**
A2D	**44**	**51**	**42**	**8.67**	**7.72**	**9.57**
A2I	**103**	**103**	**83**	**20.31**	**15.60**	**18.91**
A2O	28	41	20	5.52	6.21	4.56
P1U	5	7	1	0.99	1.06	0.23
P1D	11	5	3	2.17	0.76	0.68
P1I	9	21	11	1.77	3.18	2.51
P1O	**88**	**85**	**84**	**17.36**	**12.88**	**19.13**
P2U	17	59	32	3.35	8.94	7.29
P2D	7	13	7	1.38	1.97	1.59
P2I	24	13	9	4.73	1.97	2.05
P2O	4	20	6	0.79	3.03	1.37
D1I	18	53	22	3.55	8.03	5.01
D2I	15	47	10	2.96	7.12	2.28
Total	507	660	439	100 %	100 %	100 %

Fig 6.3.Efficiency values for P1D detector

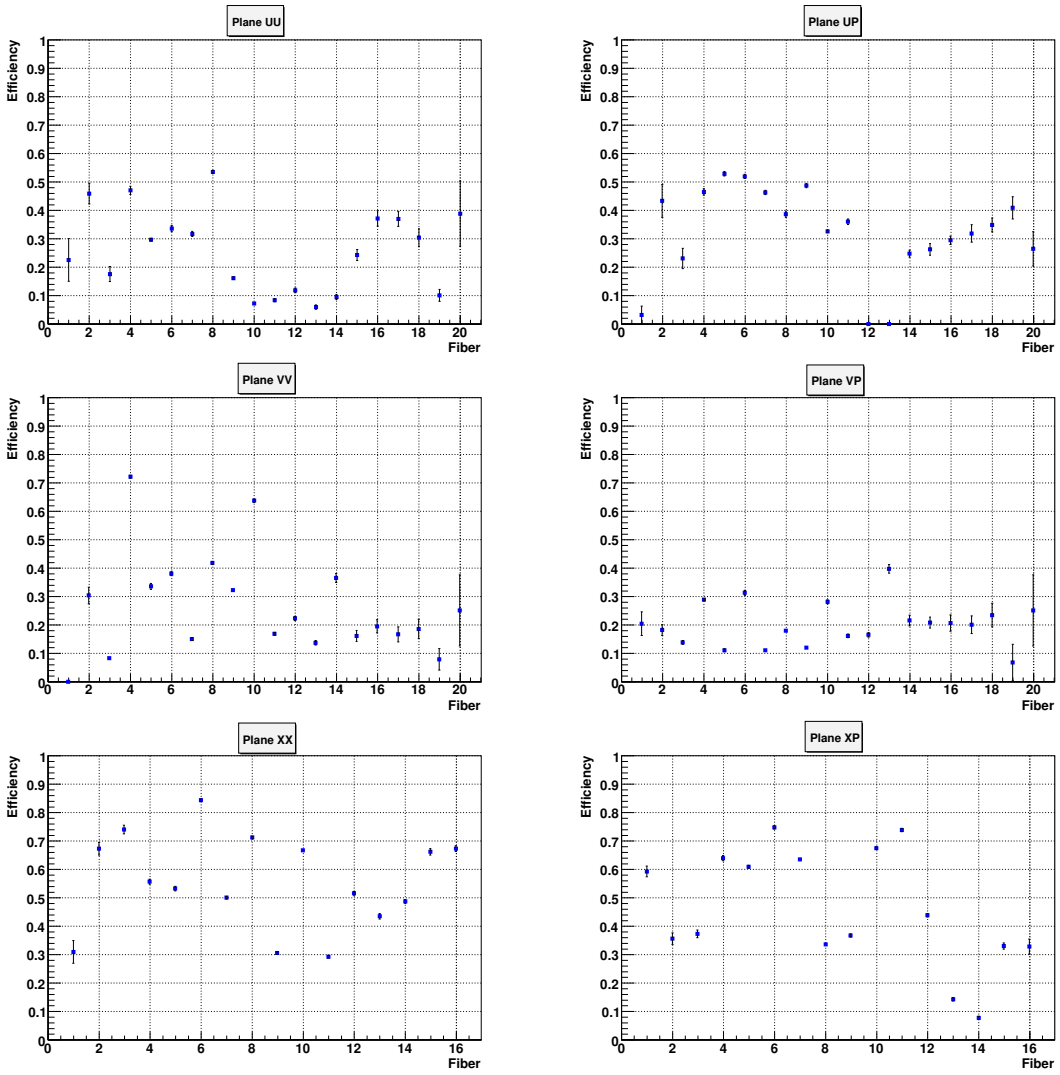

Fig 6.4.Efficiency values for A1U detector

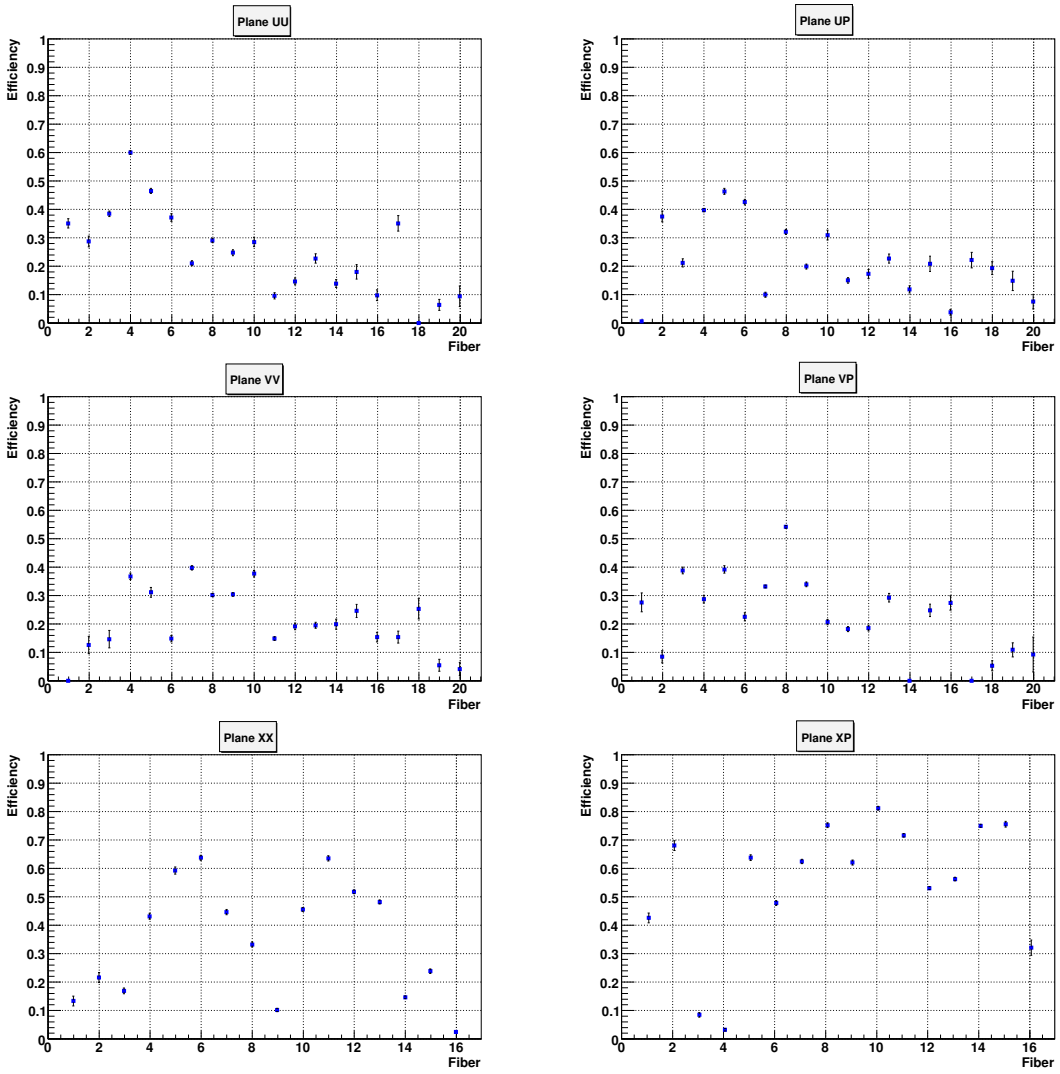

Fig 6.5.Efficiency values for A2I detector

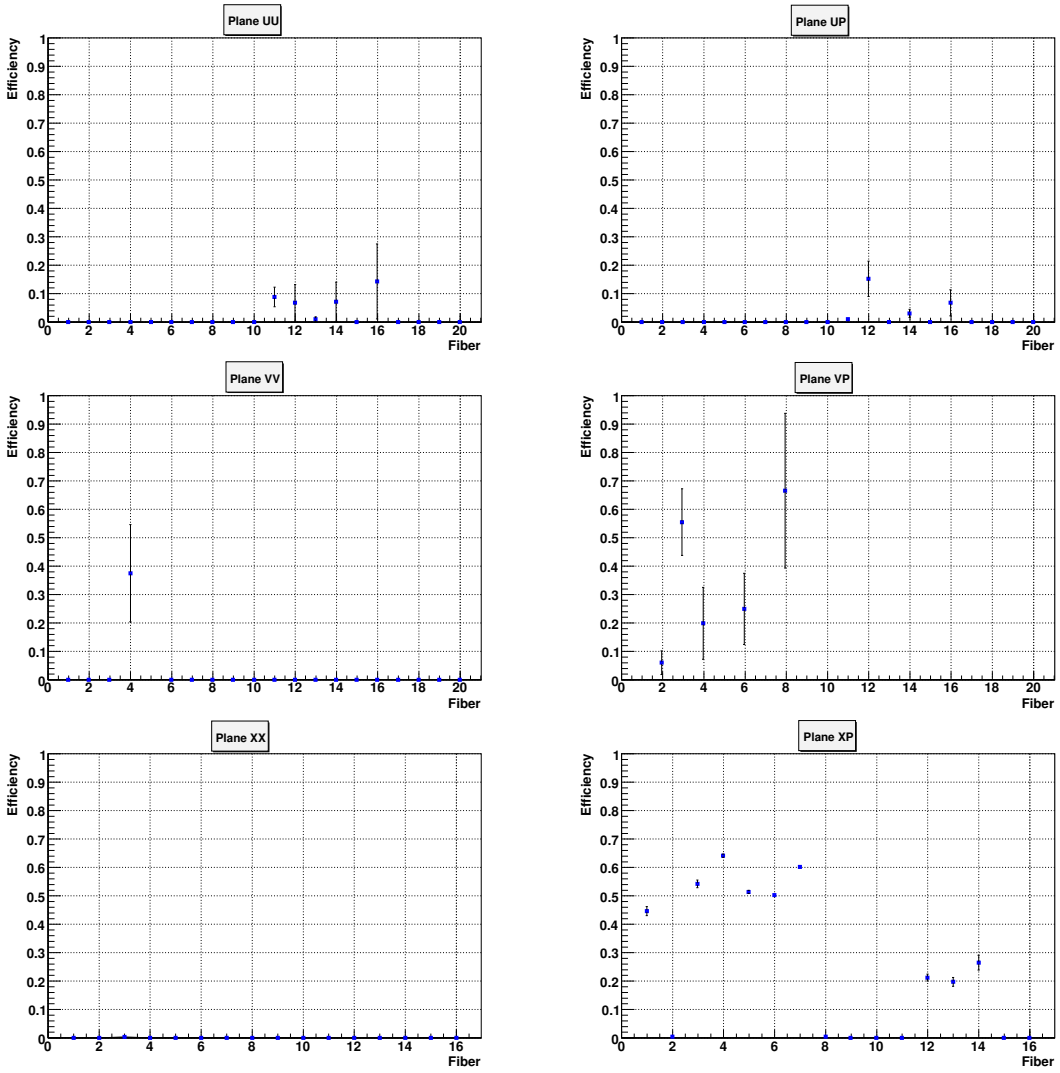

Fig 6.4.Efficiency values for A1O detector

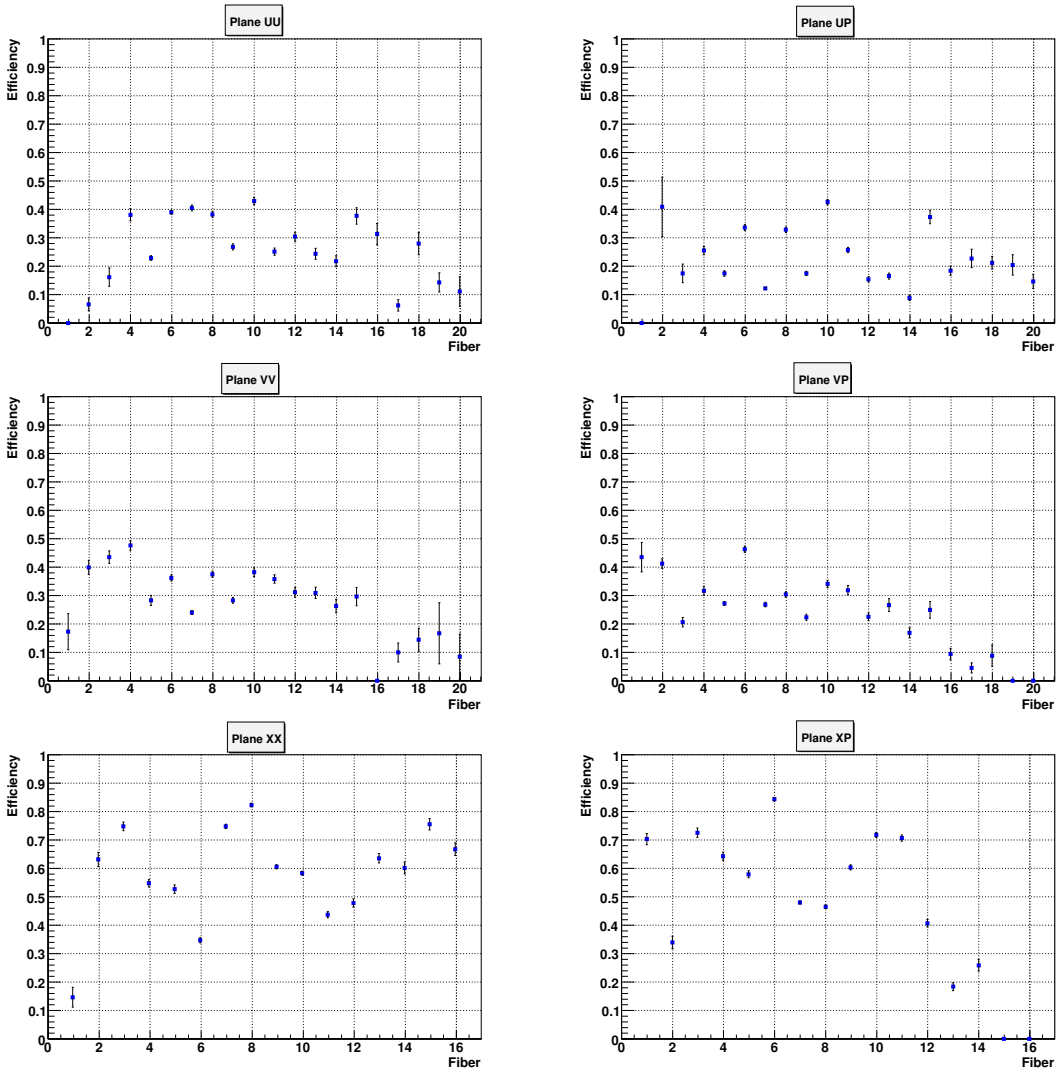

Table 6.3.EFFICIENCIES

EFFICIENCY PERCENTAGE VALUES %	**BRASIL** $\%$	**TEST 1** $\%$	**TEST 2** $\%$
Zeros on efficiency (ε)	25.15	32.74	21.78
ε <10	10.32	16.86	13.99
$10 \leq \varepsilon < 20$	12.35	22.07	18.6
$20 \leq \varepsilon < 30$	14.24	12.15	16.37
$30 \leq \varepsilon < 40$	11.36	7.94	11.21
$40 \leq \varepsilon < 50$	9.13	4.41	7.69
$50 \leq \varepsilon < 60$	7.59	2.23	4.51
$60 \leq \varepsilon < 70$	4.51	1.19	3.03
$70 \leq \varepsilon < 80$	3.07	0.25	1.98
$80 \leq \varepsilon < 90$	1.79	0.09	0.79
$90 \leq \varepsilon < 100$	0.4	0	0.05
100	0.09	0.04	0

Table 6.3 shows a summary of the different efficiency values (in percentages fo all the fibers 2016). Comparing the Brasilian results with our results it is clear that both analysis indicate that the efficiency values are lower than the expected values, because the percentages of efficiency are in a great quantity less than 50 $\%$. In other scintillating fiber detectors like the $H1$ in $HERA$ they also obtained efficiency values of this order.

CORRELATION FOR DIFFERENT NUMBER OF ENTRIES

We made a study with different number of entries to the program FIBEF.C. It is important to mention that the results for the majority of the detectors, planes and fibers are correlated in a great percentage. In figure 6.3 we can observe that the major density of points are located in efficiency values that are lower than 0.5 ($50\,\%$).

CORRELATION FOR DIFFERENT PEDESTAL FILES

We also tested the result of efficiency values for different pedestal files. For this analysis 10.000.000 of entries were used. In first place the efficiencies are determined with only one pedestal file (February pedfile) and after with two pedestal files (April and February pedfiles). Then the correlation for efficiency values is shown in figure 6.8.

With this analysis we are confident that different pedestal files don't affect in a great percentage the efficiency values. Also it is shown in Figure 6.7 that for different number of entries the efficiency values remain consistent and then the program FIBEF.C for high statistics can guarantee that the efficiency values don't depend of the number of entries, the high statistics only guarantee that the error bars are smaller.

Fig 6.7.Correlation for different number of hits

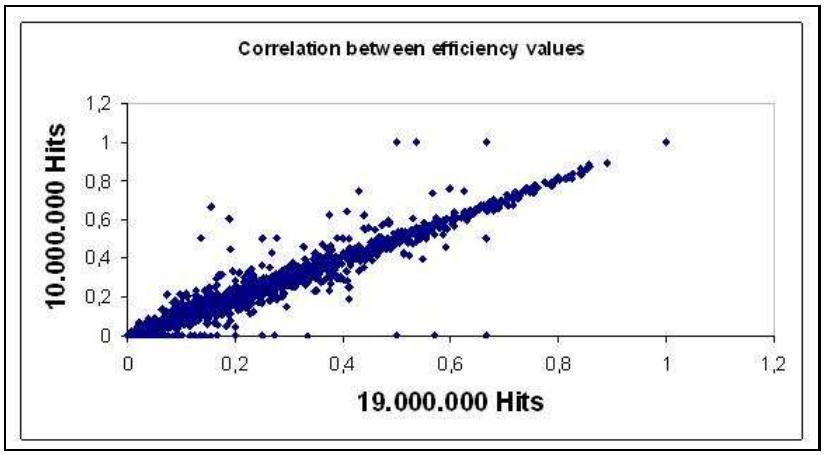

Fig 6.8.Correlation for different pedestal files

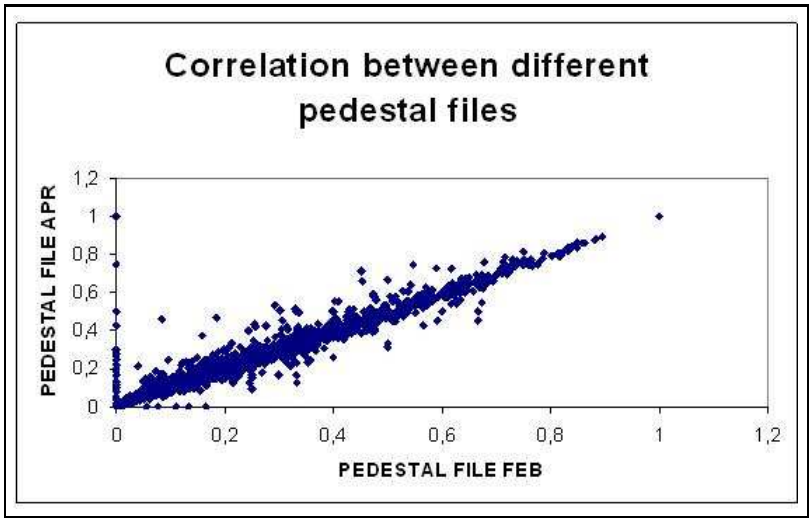

Capítulo 7

7. ANALYSIS OF ELASTIC EVENTS

The data used in this analysis were taken in Tevatron store 4647 called the $HIGH\ \beta\ STORE$. Because the Tevatron lattice conditions were different than for normal stores (this means that magnetic field intensity were different).

All the tools explained in the first chapters of this document applied to obtain our results. For this reason it was important to understand these tools to give at the end of the work conclusions about the quality of the data sample, which could make possible a future measurement of the elastic differential cross section at center of mass energy of $\sqrt{s} = 1{,}96$ TeV on the interval of four momentum transfer of 0.2-1.5 GeV^2 with all the necessary corrections.

7.1 ANALYZED EVENTS

For this part of the analysis events contained in the RUNS 215445 to 215449 were used, this is around 6 million of events. The first cut applied was to only allow to pass the elastic triggers called ELAS, and ELAS2. ELAS triggered selected events that had 3 fiber segments in each of the 4 detectors that make an elastic combination for example A1U, A2U, P1D and P2D detectors for the AU-PD elastic combination. ELAS2 was a less restrictive trigger that allowed to have only 2 out of 3 fiber segments in the second detectors making the elastic trigger. All the cuts following the analysis are inserted in a routine called ELAS1.H which is the header file of the program ELAS1.C that has all the information of elastic events that going to be treated and analyzed in this chapter.

Continuing with the trigger analysis, the trigger ELAS accepts events only if the events hit the four detectors of the elastic combination. For example $A1U$, $P1D$, $A2U$, $P2d$ while the trigger ELAS2 only accepts events with two detector of the elastic combination, for example $A1U$ and $P1D$. In the table showed below are the number of events accepted for these two triggers:

Table 7.1 Triggers

TRIGGER NUMBER	TRIGGER NAME	EVENTS
37	ELAS	240534
70	ELAS 2	1111124

In the figure 7.1 is indicated the total statistics of events and are tagged the elastic triggers 37 and 70.

Fig 7.1.Trigger distribution

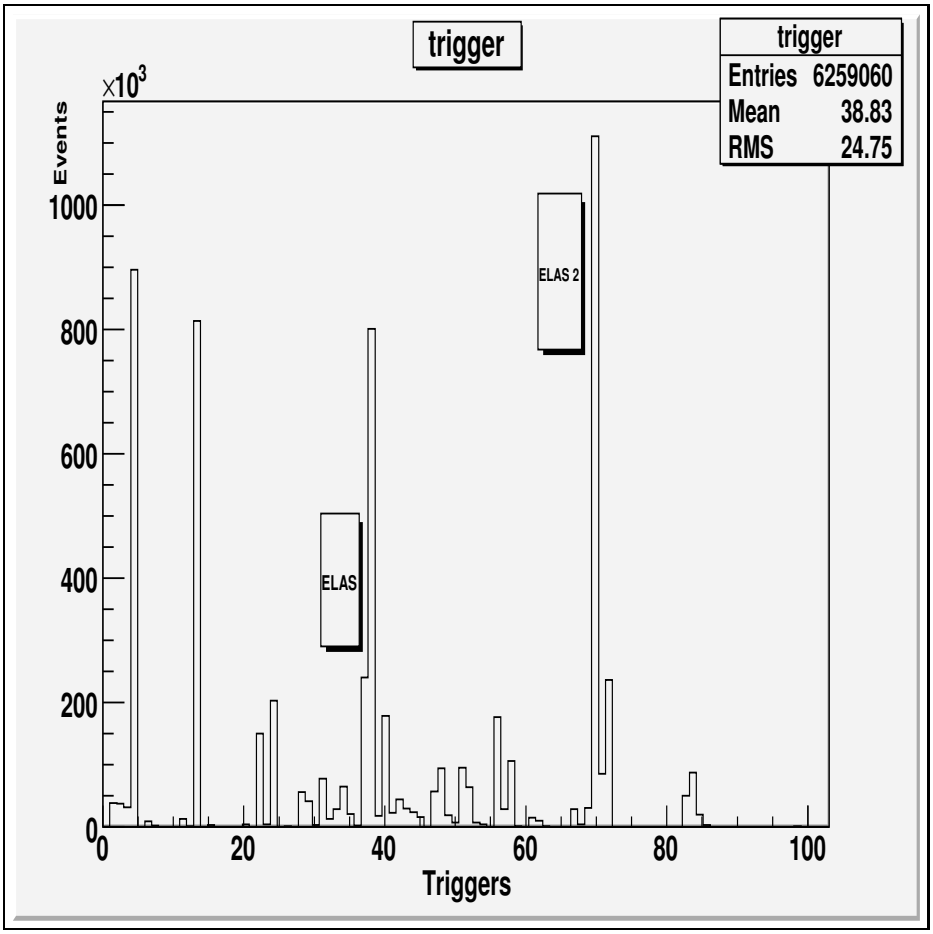

Table 7.2.Roman pot positions with respect to the beam

POT POSITIONS			
POT	POS_{beam} (mm) DATASET 1	POS_{beam} (mm) DATASET 2	ΔPOS (mm)
A1U	5.75	5.41	0.34
A1D	5.44	4.08	1.36
A1I	3.83	3.83	0.00
A1O	14.74	12.21	2.53
A2U	4.53	4.24	0.29
A2D	5.04	5.04	0.00
A2I	4.02	4.37	-0.35
A2O	12.52	10.27	2.25
P1U	9.17	7.96	1.21
P1D	5.7	3.88	1.82
P1I	11.00	9.22	1.78
P1O	8.11	3.83	4.28
P2U	8.17	7.11	1.06
P2D	4.94	3.87	1.07
P2I	11.72	10.2	1.52
P2O	4.39	4.39	0.00

7.2 POT POSITIONS

There were mainly two sets of pot positions with high statistics which are listed in table 7.2, at the moment we have been working with the set of runs that have the closest detector positions with respect to the beam.

7.3 HIT RECONSTRUCTION

For this analysis a fiber is considered to be on if its ADC counts are over a threshold which is defined as:

$$MeanPedestalValue + 4 * \sigma_{pedestal} + Disc \tag{7.1}$$

where Disc is a discriminator applied that has a value of about 30 counts.
Once we decide if one fiber fires in a specific plane we check if there is an adjacent fiber in the primed plane to define the fiber segment where the particle went trough. If there are multiple fibers fired, we end up with a list of fiber segments per plane.

For this work it is required at least 2 fiber segments reconstructed per detector and the intersection of them give the X, Y coordinates of the hit as it was explained in chapter four. Then we make a list of all possible hits in the analyzed detector. The hits are weighted by the sum of ADC counts of all

the fibers that contributed in the reconstruction of the hit. For the analysis we allow a maximum of 3 fibers firing per scintillating fiber layer and we are picking up in the analysis the hit in the event with highest sum ADC weight.

We have tried other definitions for the hit but we have ended up with the definition that maximizes the number of elastic events picked up at the end.

Figure 7.2 shows the comparison of the X coordinate obtained from U-V fiber segments compared to X segment coordinate for all the detectors of the Forward Proton Detector, the difference allow us to determine the detector resolution.

Table 7.3 shows the detector resolution found for each of the 18 FPD detectors in our analysis.

Fig 7.2.Resolution for all the detectors

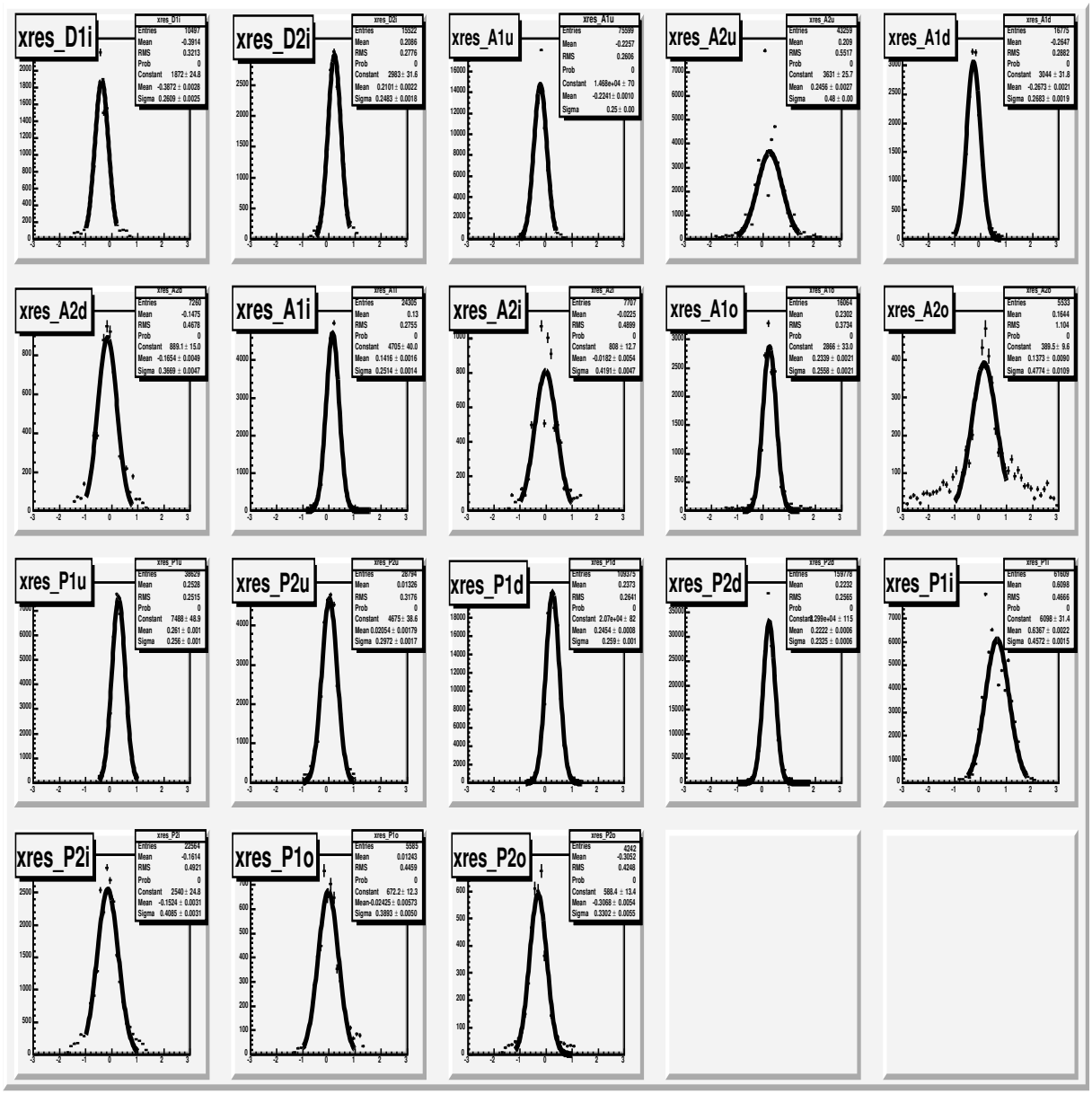

Table 7.3.Resolution obtained from $X_{uv} - X_x$

DETECTOR RESOLUTION			
DET	MEAN (mm)	STDEV (mm)	$\sigma(\mu m)$
A1U	-0.224	0.250	166
A1D	-0.267	0.268	180
A1I	0.142	0.251	170
A1O	0.234	0.256	166
A2U	0.246	0.48	276
A2D	-0.165	0.367	228
A2I	-0.018	0.419	266
A2O	0.137	0.477	240
P1U	0.261	0.256	152
P1D	0.245	0.259	177
P1I	0.637	0.457	322
P1O	-0.024	0.389	257
P2U	0.021	0.297	197
P2D	0.222	0.232	180
P2I	-0.152	0.408	252
P2O	-0.307	0.330	216

7.4 DETECTORS PERFORMANCE

Now we show the correlations between primed and unprimed layers in each detector by plane. All fibers above threshold are plotted for events that have a single validated hit in both detectors. The expected correlation between fibers can be seen, where the fiber number is either the same in both layers or shifted by one. Some additional uncorrelated “noise” can be observed.

The correlation band indicates that the signal from the system is consistent with real particles passing through the detectors. With help of all these correlations it is shown that the detectors most affected are the A2U, A2D, A2I and this shows that there exist a correlation with the efficiency study. The advantage of this kind of analysis is that it give us an idea to how is the real performance of all the FPD detectors and also show us where there are problems.

Fig 7.3.Correlation for A1 Castle

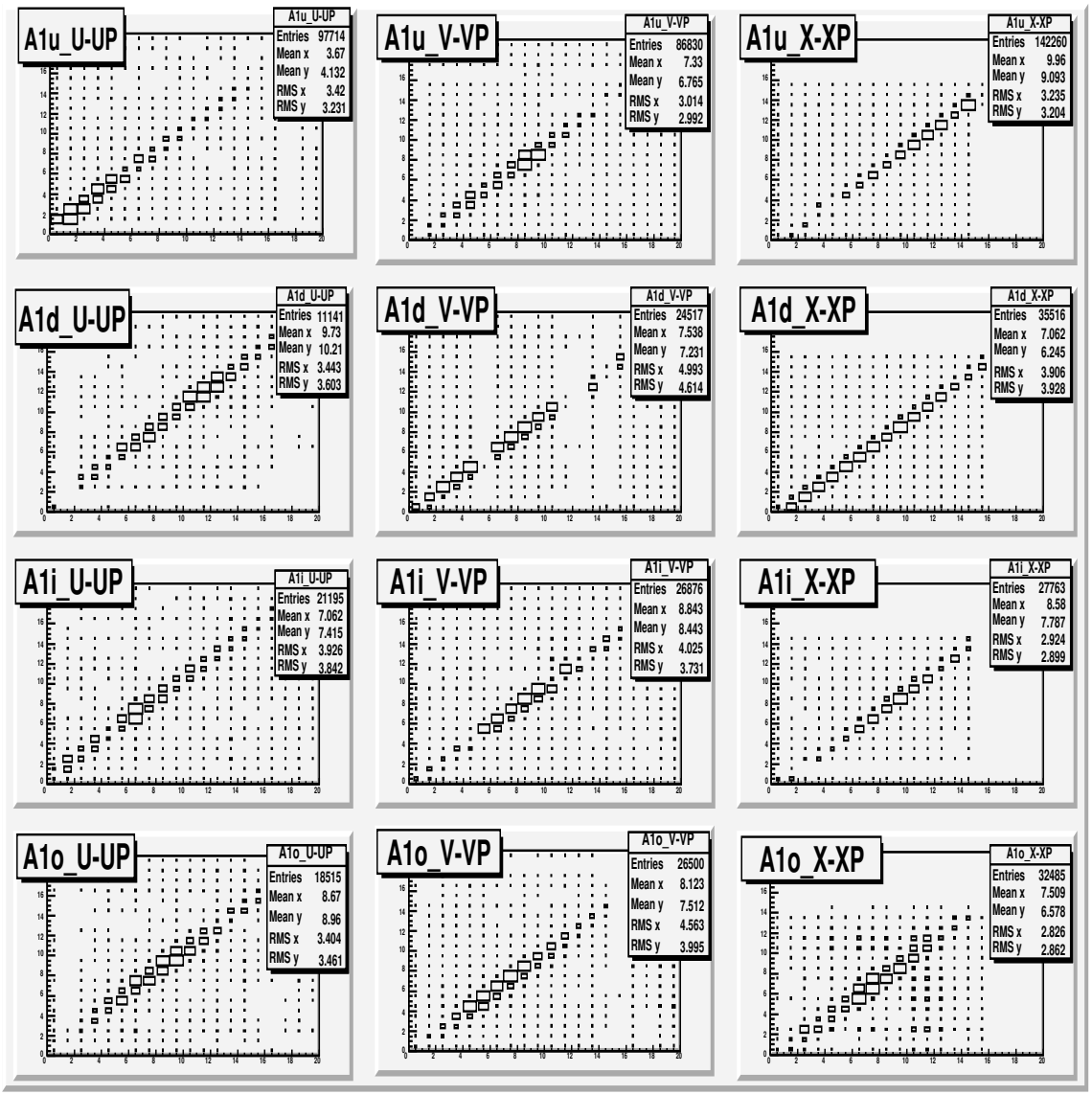

Also with the help of the study of the detectors performance we can find a list of dead fibers that is shown in table 7.4. If we compare the detectors with most dead fibers and the detectors with zero efficiency we find that there exist a correlation because the majority of the dead fibers are present in the same detectors that have less efficiency values. Then we conclude that for future analysis a softawre can be developed to relate the dead fibers with efficiency determination.

Fig 7.4.Correlation for A2 Castle

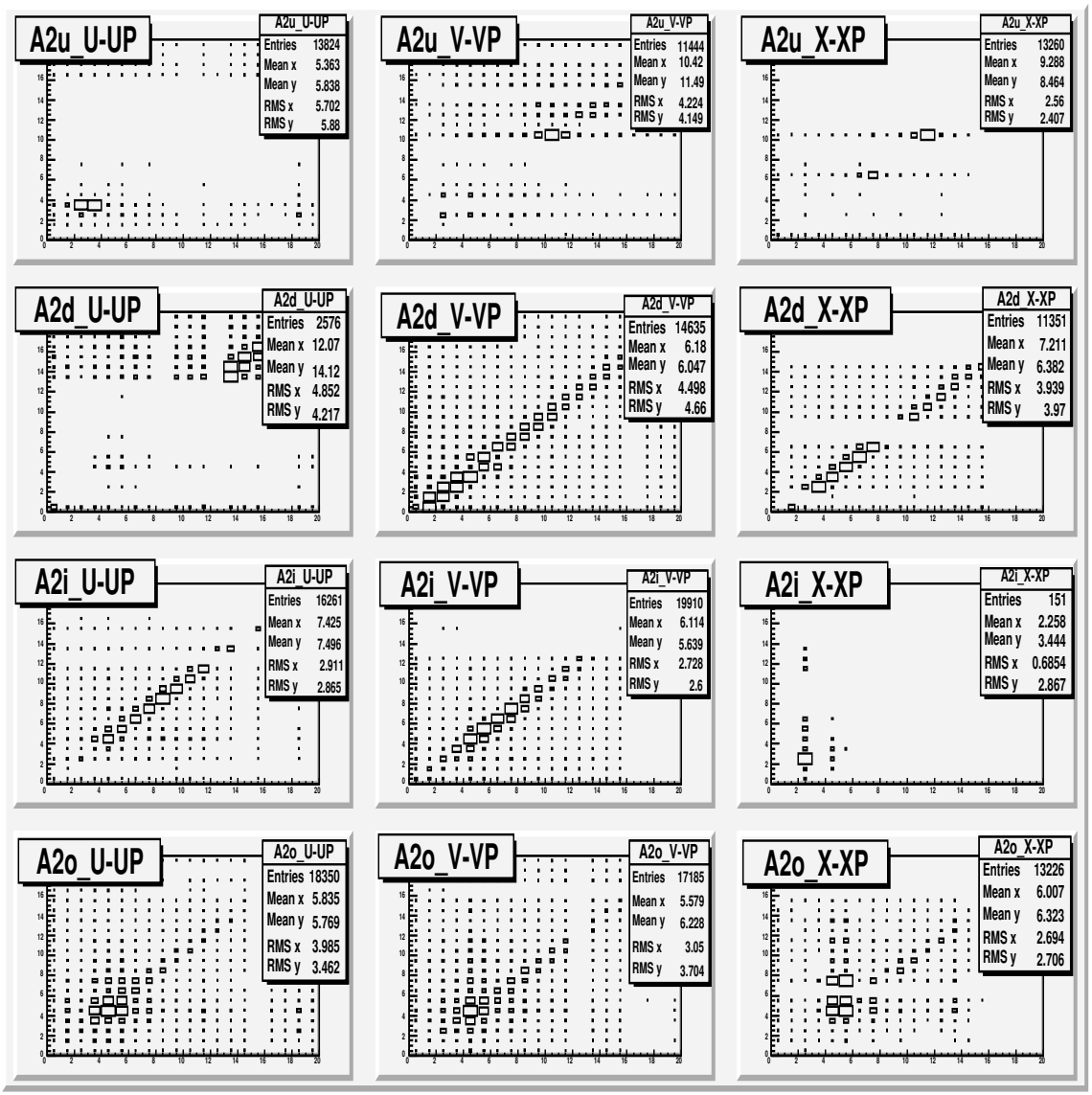

Fig 7.5.Correaltion for P1 Castle

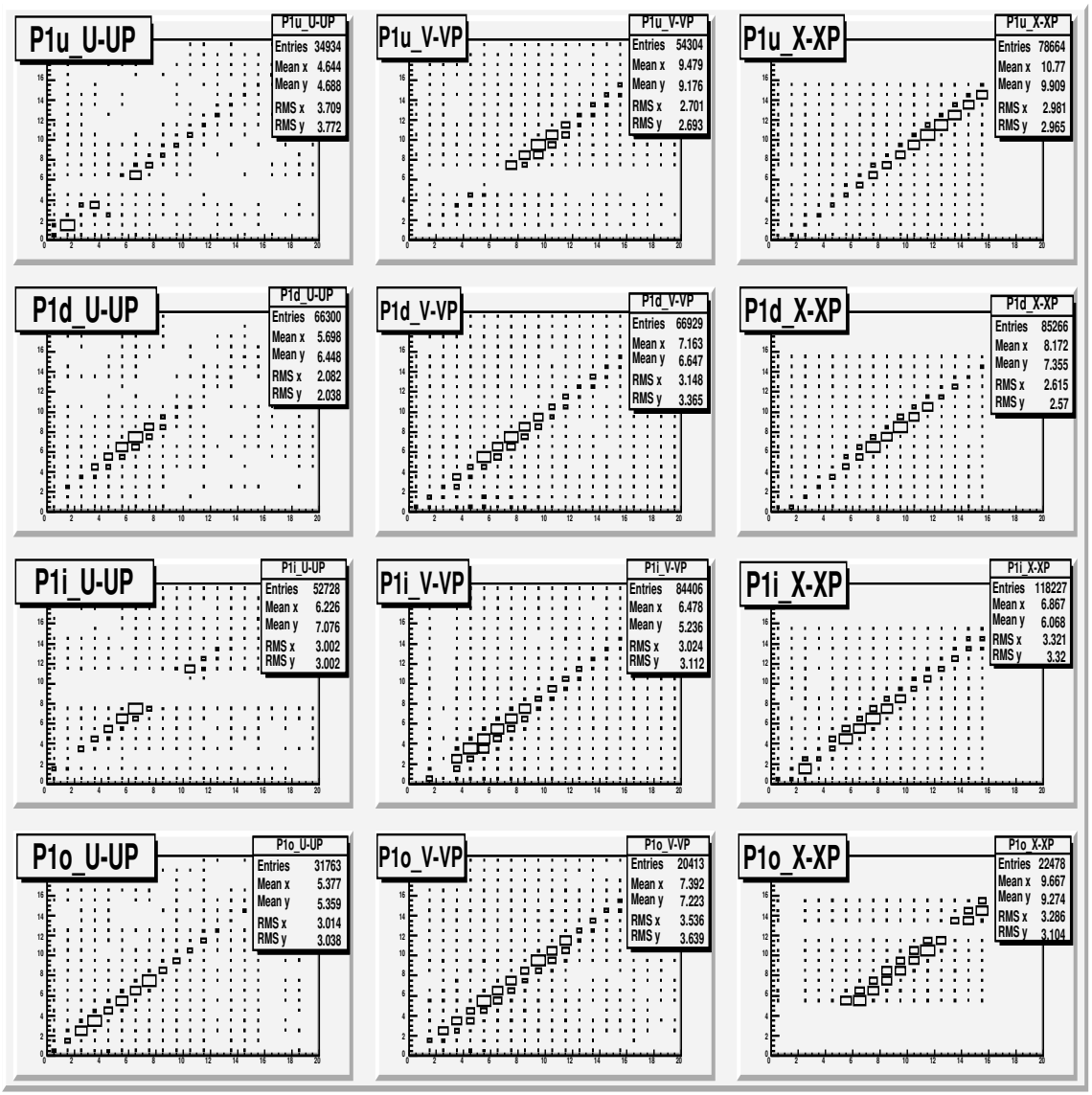

Fig 7.6.Correlation for P2 Castle

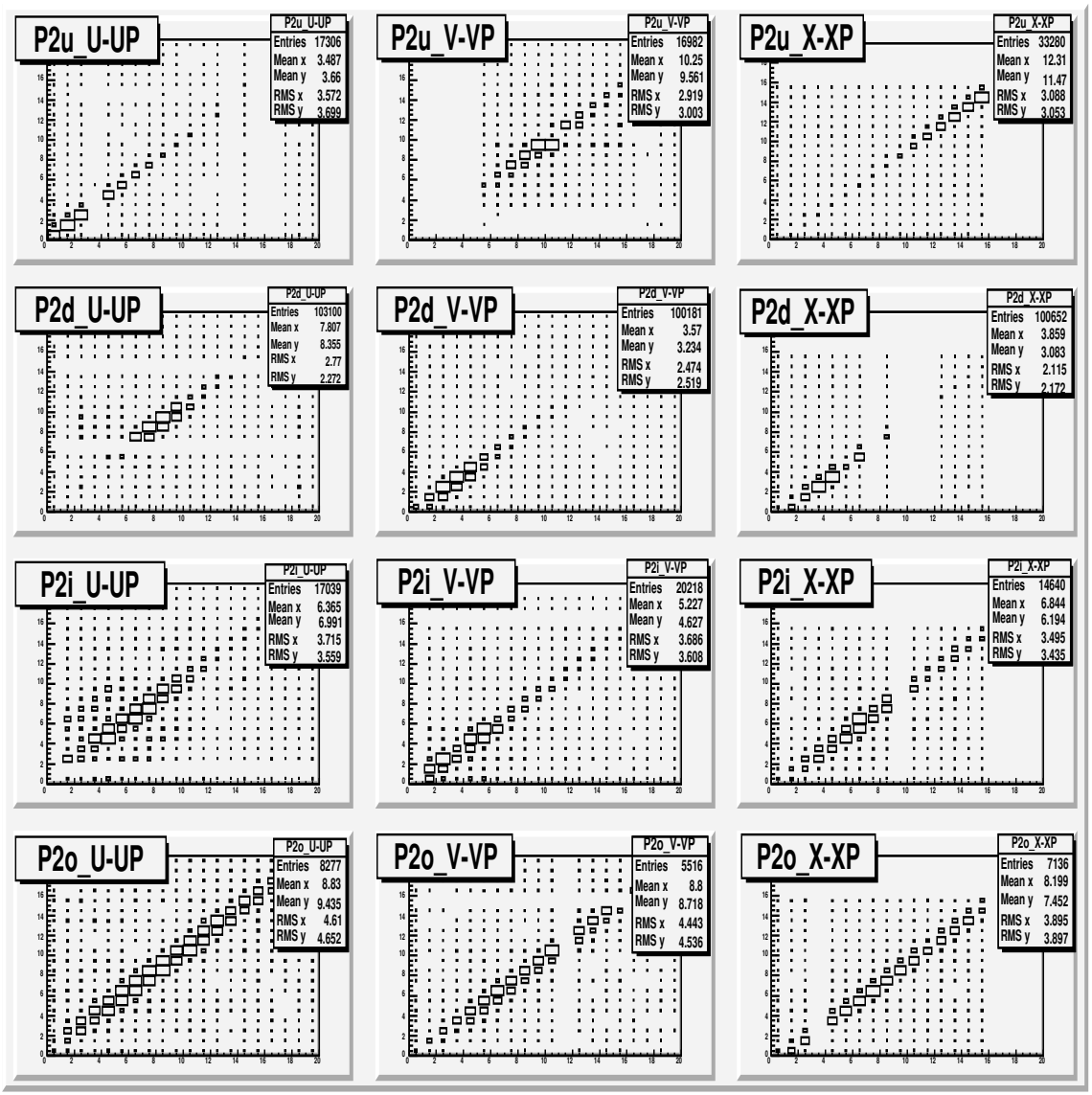

Table 7.4.Dead fibers

DEAD FIBERS LIST						
DET	**U**	**U'**	**V**	**V'**	**X**	**X'**
A1U	17			16	15	
A1D	17		5,11,12,14			
A1I						
A1O	16,19	13	15	18		14,15
A2U	10	0-2,4-15		6,7,8	15	0-3,7-9,11-15
A2D		0-12	15			7,8
A2I	14-17,19	12,16-19	16-19	16-19	0-16	0-16
A2O	15	18	12,16,17	16	15	6
P1U		5		5,6		
P1D		11,12				
P1I	13	8,9,10	0,1,2			
P1O	16					0-4,12
P2U	3,13,15,16		0-4,17			
P2D		6,14			5,7,9-11	
P2I				16	9	
P2O			11			3

7.5 ELASTIC EVENT CANDIDATES

To select the data used in this section it is required that there exist hits in both detectors that make up a spectrometer combination and then proceed to plot the X,Y coordinates for both detectors.

We can see a definite band from real particles going trough the spectrometer, but on top of that also we can see some uncorrelated events which are background.

BACKGROUND

Different types of false impacts exist in the detector associated to background that must be considered:
1. Halo: Corresponds to the particles outside of the central nucleus of the beam that can hit the detectors of the FPD and they turn out to be indistinguishable from the elastic particles that come from the interaction point.
2. Collisions with gas: Protons and antiprotons which have been scattered from the main bunch due to interactions with surrounding particles of residual gas. These generate multiple hits in the detector.
3. Multiple Interactions: More than one proton-antiproton collision when the bunches collide at the interaction point.
4. Noise: Another background type that is associated to electronic noise of the different components of the detectors.

Fig 7.7 shows the x coordinates correlation for the PD and AU spectrometers and figure 7.8 shows the correlations in the y coordinates.

Fig 7.7.X2 vs X1 correlation plots for PD and AU detectors

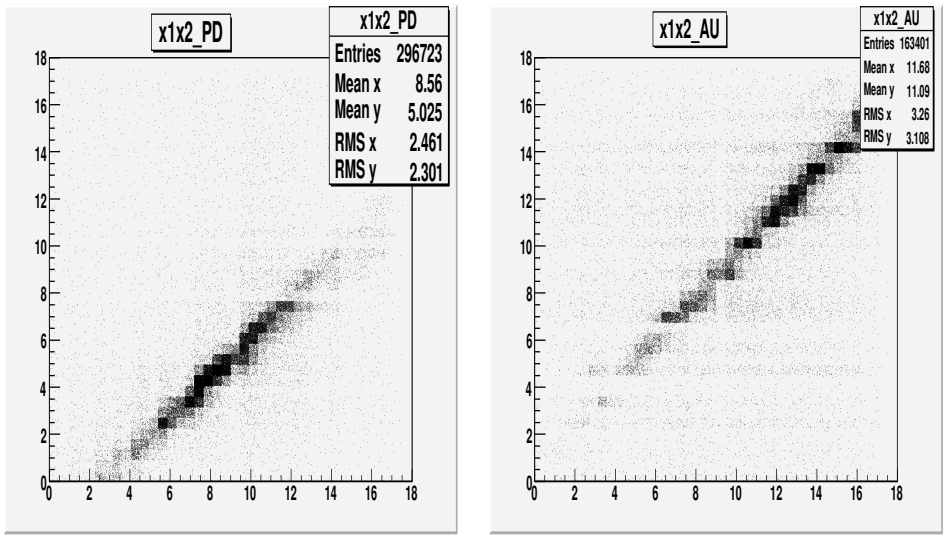

Fig 7.8.Y2 vs Y1 correlation plots for PD and AU detectors

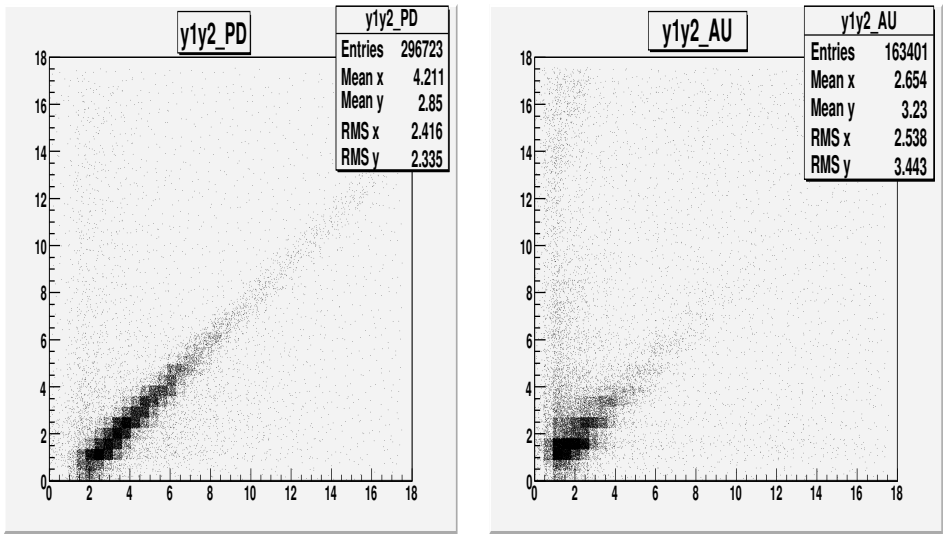

We require band cuts to select only the events inside the diagonal band correlations and then request that the opposite side spectrometer should also have a hit with coordinates inside the spectrometer correlation band. In figures 7.9 and 7.10 it be verified that we have elastic events properly selected because we see the correlation between coordinates for the $\overline{p}$ and proton spectrometers. To select elastic events and make cuts on the different correlations we just measure the y coordinate from the bottom of the detector and the x coordinate from the corner that corresponds to x fiber number 1.

Also it is shown in figures 7.11 and 7.12 the correlation of the four possible combinations: AUPD, ADPU, AIPO, AOPI, before and after the cuts on the elastic bands, these figures show that the elastic cuts made are correct.

One way to study elastic events is trough of the coordinates correlation "scatter plot" in the detectors, in other words, plot $x1$ vs $x2$ and in a similar way for y coordinates, in figures 7.7 and 7.8 we show this type of correlation, in these figures it is observed the contamination.of non elastic events which are outside of the diagonal, this type of events may occur due to the following reasons:

A. Contamination due to diffractive events that correspond to the events outside of the diagonal
B. Into the diagonal also there is contamination due to events of beam halo.

Fig 7.9.X2 vs X1 correlation plots for each FPD spectrometer

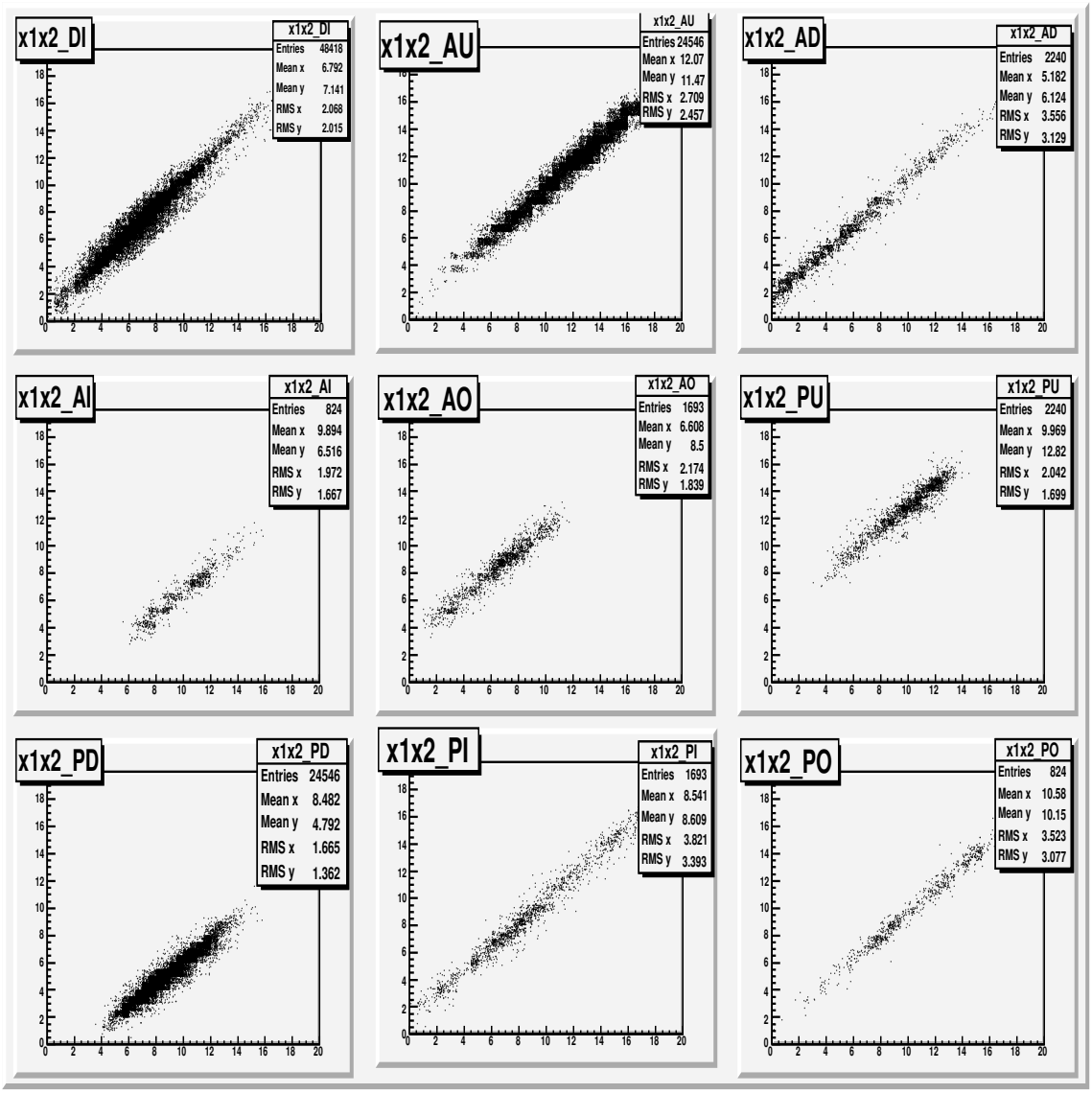

Fig 7.10.Y2 vs Y1 correlation plots for each FPD spectrometer

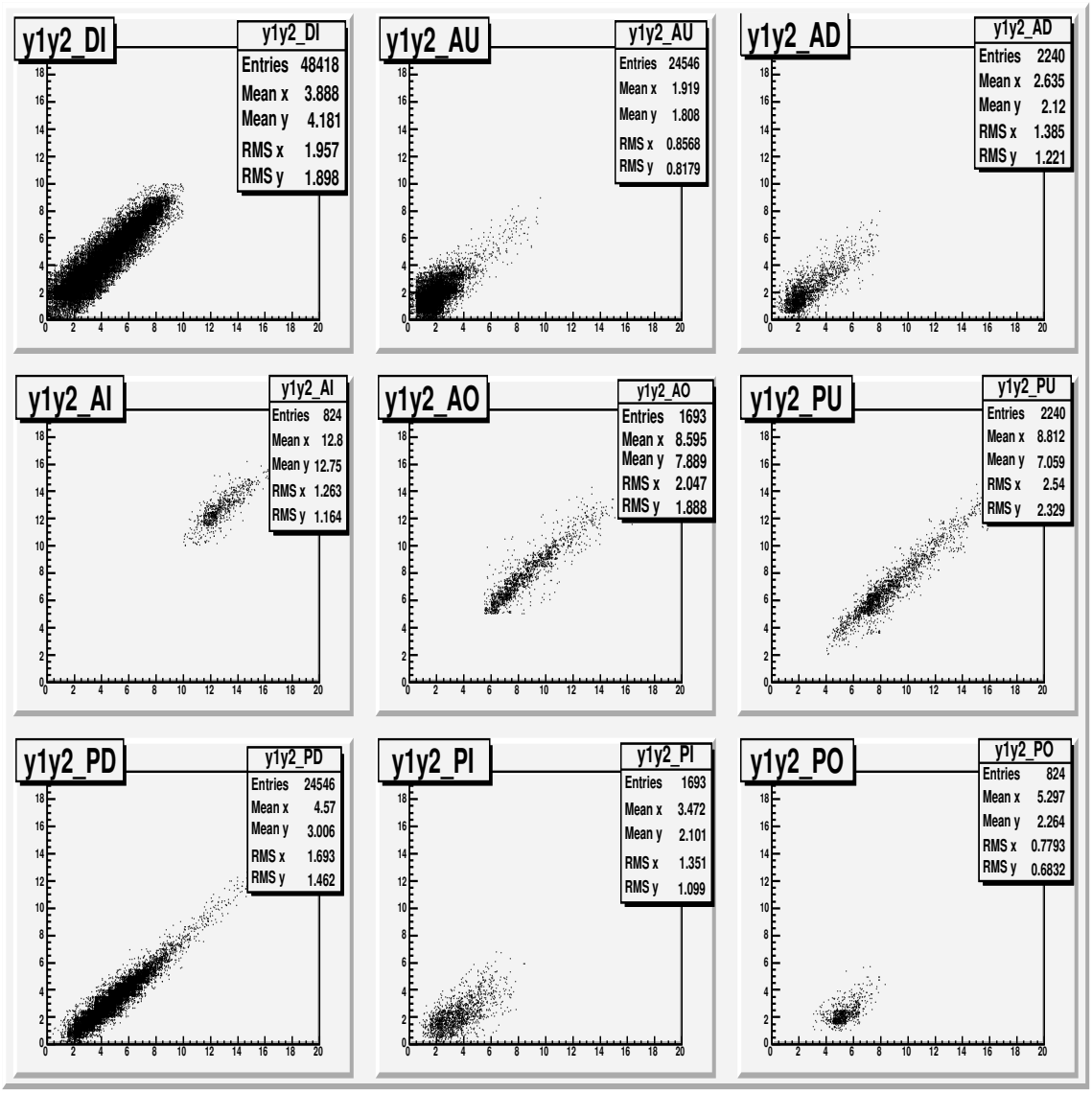

Fig 7.11.X2 vs X1 correlation plots for PD and AU detectors

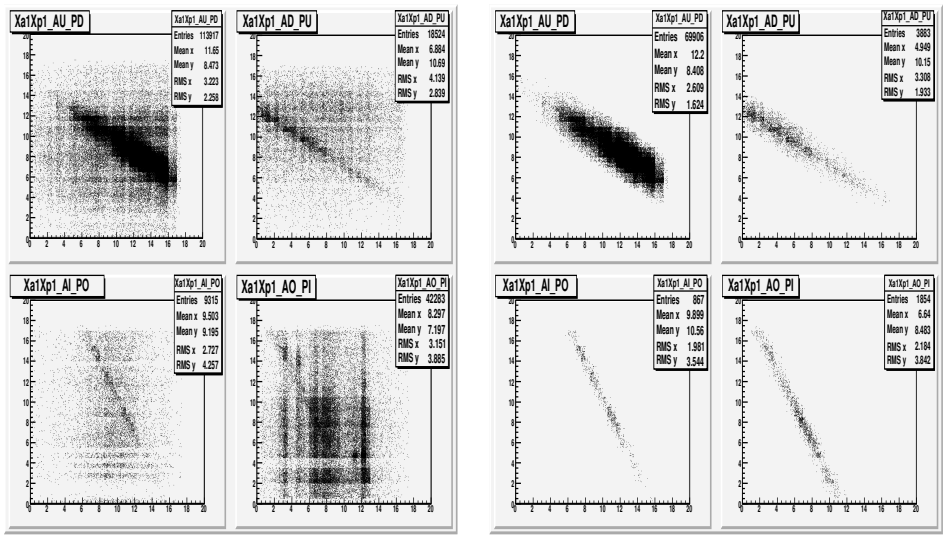

Fig 7.12.Y2 vs Y1 correlation plots for PD and AU detectors

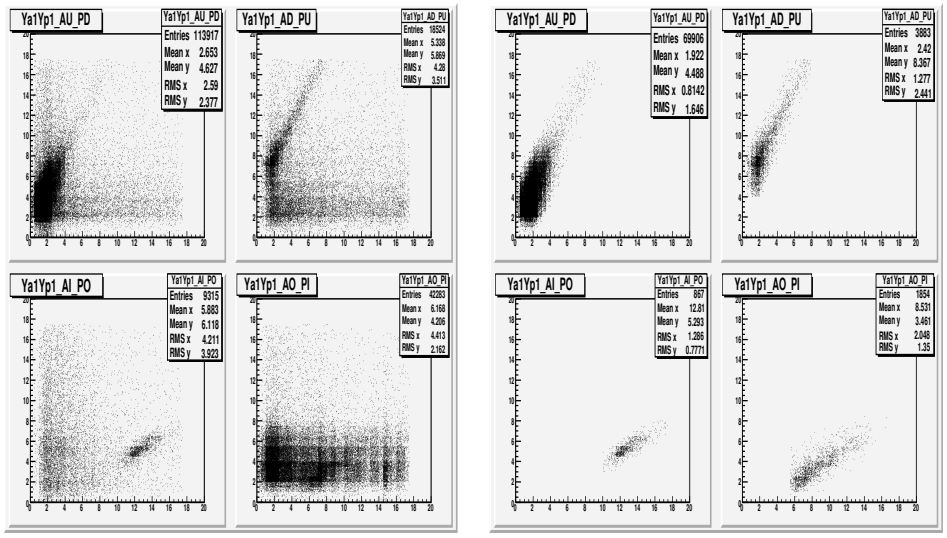

The elastic event selection can be made without worring about the actual location with respect to the particle beam. Therefore, for the elastic event selection we can use the coordinates with respect to the detectors. To obtain the scattering angle, and any other kinematic variable, it is necessary to know the location of the detectors with respect to the beam, then with this information we can translate the coordinates measured from the detector reference to the particle beam reference.

Fig 7.13.Elastic events

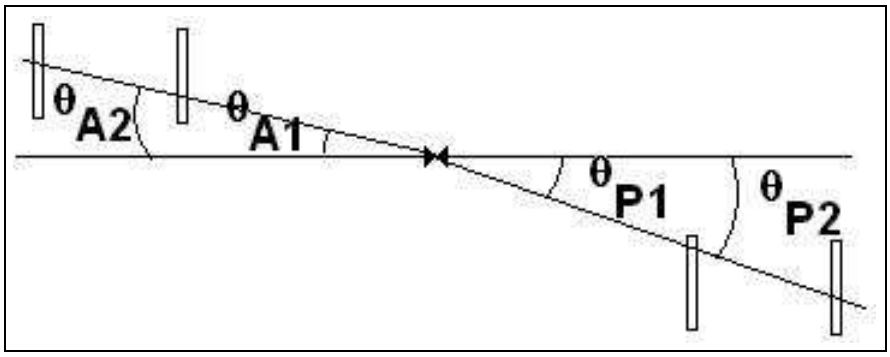

Then with consistent correlations for different spectrometers finally the detector is alligned with respect to the particle beam. To do this we find the beam offset in X with respect to the center of P1D and P2D detectors and the beam offset in Y with respect to the center of A1O and A2O detectors. All other beam offsets can be automaticallly obtained if an elastic sample is used given the fact that the reconstructed interaction point offset and scattering angle as is showed in the figure 7.13 should be the same for both $\overline{p}$ and proton spectrometers that make part of the elastic combination.

Figure 7.14 shows the gaussian fits performed to the X distribution of each detector, we just use the center of the X distributions for A1O, A2O, P1D and P2D detectors which show to be the best fits.

Tables 7.5 and 7.6 show the beam offsets obtained by using the different elastic combinations.

We take the average over all 4 elastic combinations as the offset of the beam at each castle location. Once the beam offsets are known it can be verified that all elastic combinations give consistent answers for the physical variables that we want to measure. Using the transport matrices for the high beta optics one can find the interaction point offset and the scattering angle at the IP, with the scattering angle we can determine the four-momentum transfer t. Because we have selected a good sample of elastic events, it is known that the momentum of the elastic scattered proton and $\overline{p}$ is 980 GeV, so the uncertainty in t only comes from the uncertainty in the scattering angle. Table 7.7 shows the values of X_{IP} and Y_{IP} obtained from each spectrometer and:

$$\Delta t = t_{\overline{p}} - t_{proton} \tag{7.2}$$

the difference in four momentum transfer obtained from the $\overline{p}$ and proton spectrometers for each of the 4 elastic combinations.

Fig 7.14.Gaussian fits to the X distributions of each FPD detector

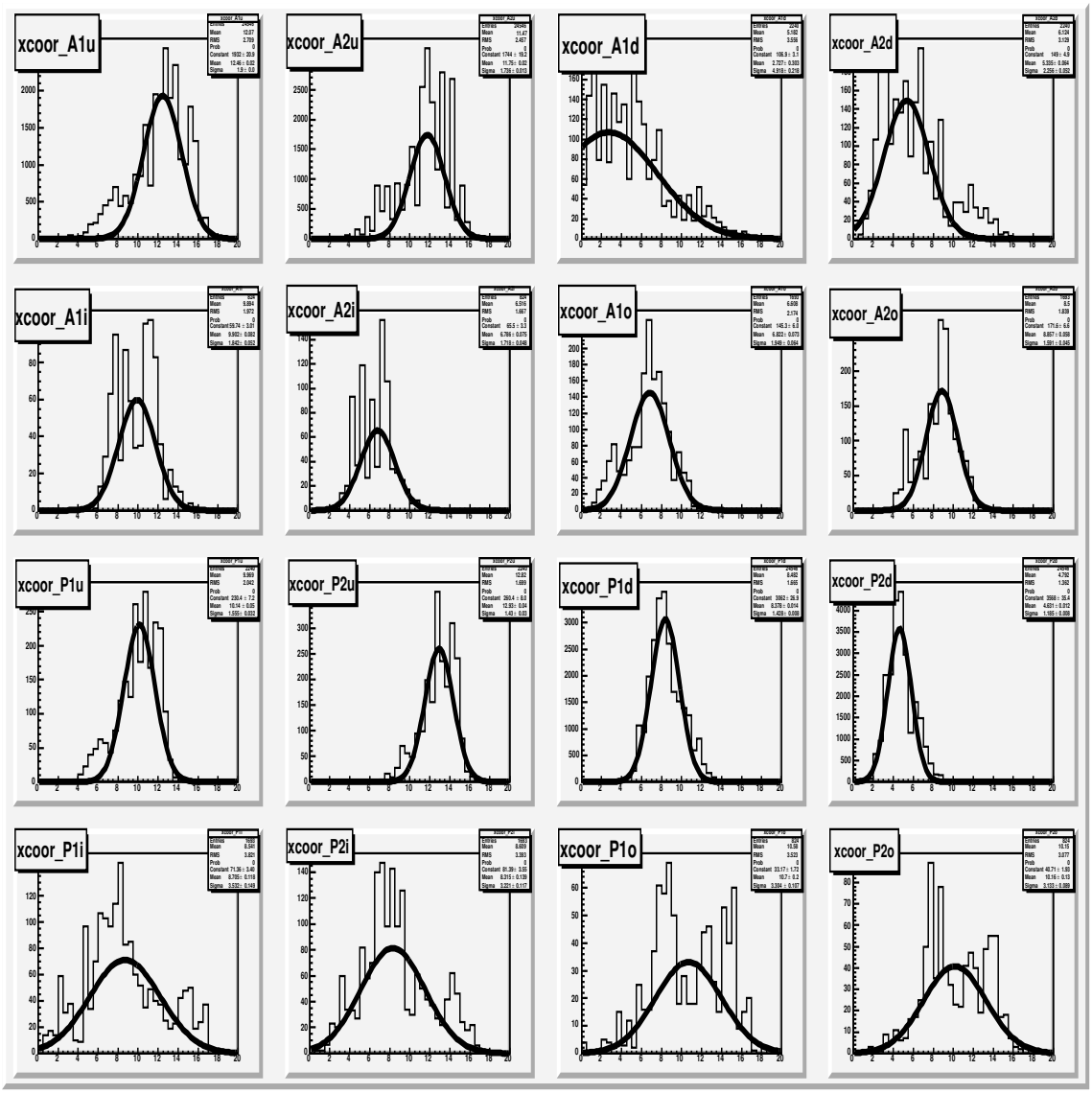

Figure 7.15 shows the IP offset distributions reconstructed from the 4 elastic combinations. We can see a perfect agreement among all 4 combinations. Figure 7.16 shows the difference in the reconstructed t from the proton and $\overline{p}$ spectrometers and finally figure 7.17 shows the $\frac{dN}{dt}$ distributions for all 4 elastic combinations and compare the t distribution from $\overline{p}$ and proton spectrometer. All the distributions show that alignment has converged.

Table 7.5.Y beam offsets

ElASTIC SAMPLE	$YA1_{offset}$ (mm)	$YA2_{offset}$ (mm)	$YP1_{offset}$ (mm)	$YP2_{offset}$ (mm)
AUPD	0.426	-2.82	3.34	2.76
ADPU	0.426	-2.82	3.26	2.68
AIPO	0.426	-2.82	3.25	2.67
AOPI	0.426	-2.82	3.36	2.80
AVERAGE	FIXED BY GAUSSIAN FIT	FIXED BY GAUSSIAN FIT	3.30 ± 0.056	2.73 ± 0.063

Table 7.6.X beam offsets

ElASTIC SAMPLE	$XP1_{offset}$ (mm)	$XP2_{offset}$ (mm)	$XA1_{offset}$ (mm)	$XA2_{offset}$ (mm)
AUPD	-0.068	-3.986	3.43	2.72
ADPU	-0.068	-3.986	4.32	3.38
AIPO	-0.068	-3.986	3.68	2.90
AOPI	-0.068	-3.986	4.26	3.53
AVERAGE	FIXED BY GAUSSIAN FIT	FIXED BY GAUSSIAN FIT	3.92 ± 0.44	3.13 ± 0.38

Table 7.7.IP offsets and Δt from 4 elastic combinations

ElASTIC SAMPLE	YIP$_{\overline{p}}$ (mm)	YIP$_{proton}$ (mm)	XIP$_{\overline{p}}$ (mm)	XIP$_{proton}$ (mm)	Δt_{mean} $(GeV/c)^2$	Δt_{rms} $(GeV/c)^2$
AUPD	0.019	0.043	-0.267	-0.265	-0.0001	0.065
ADPU	0.031	0.033	-0.259	-0.238	0.0076	0.059
AIPO	0.032	0.046	-0.309	-0.258	0.018	0.052
AOPI	-0.012	-0.009	-0.264	-0.205	-0.004	0.0077
AVERAGE	0.017 ± 0.020	0.028 ± 0.025	-0.27 ± 0.023	-0.24 ± 0.026		

Fig 7.15.Reconstructed IP offsets

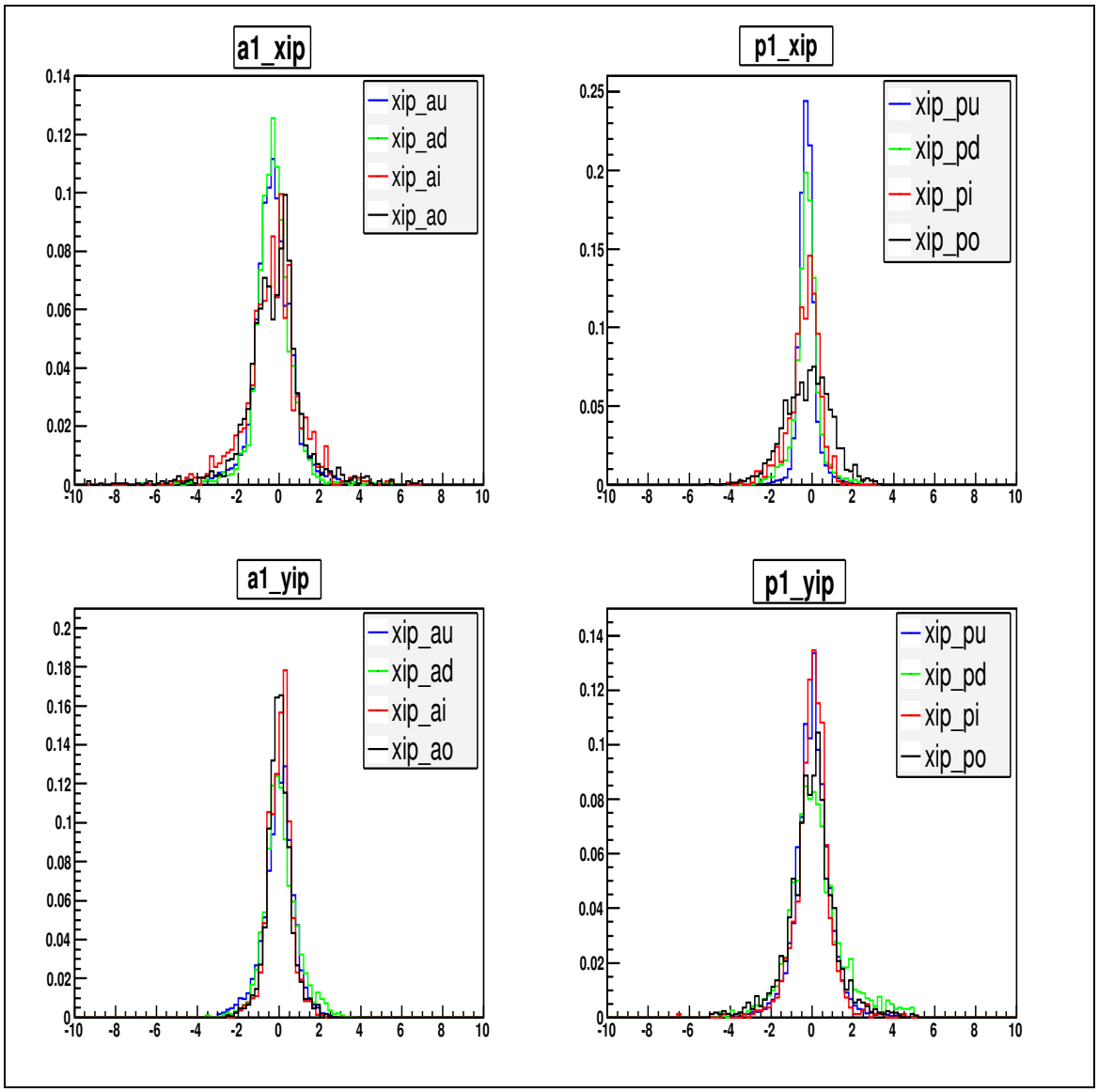

Fig 7.16.Difference in the reconstructed t

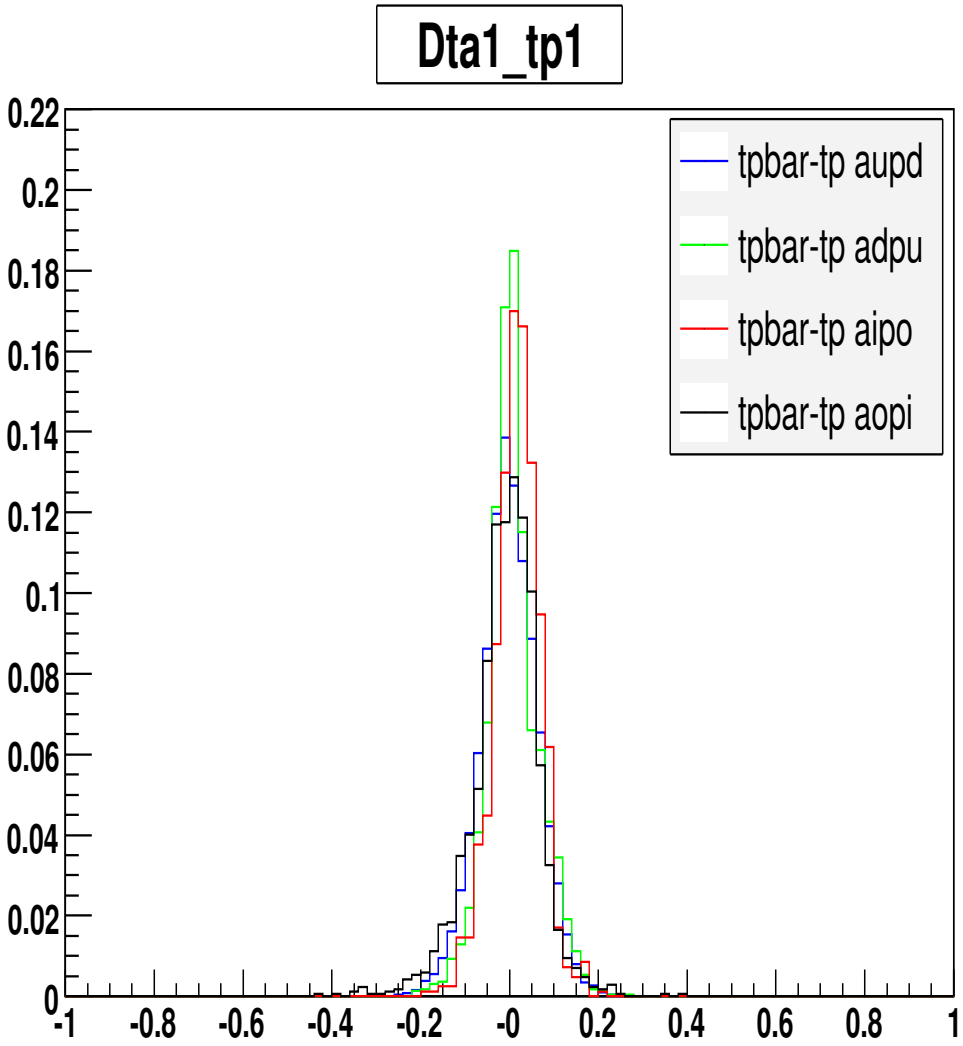

Fig 7.17.Reconstructed $\frac{dN}{dt}$

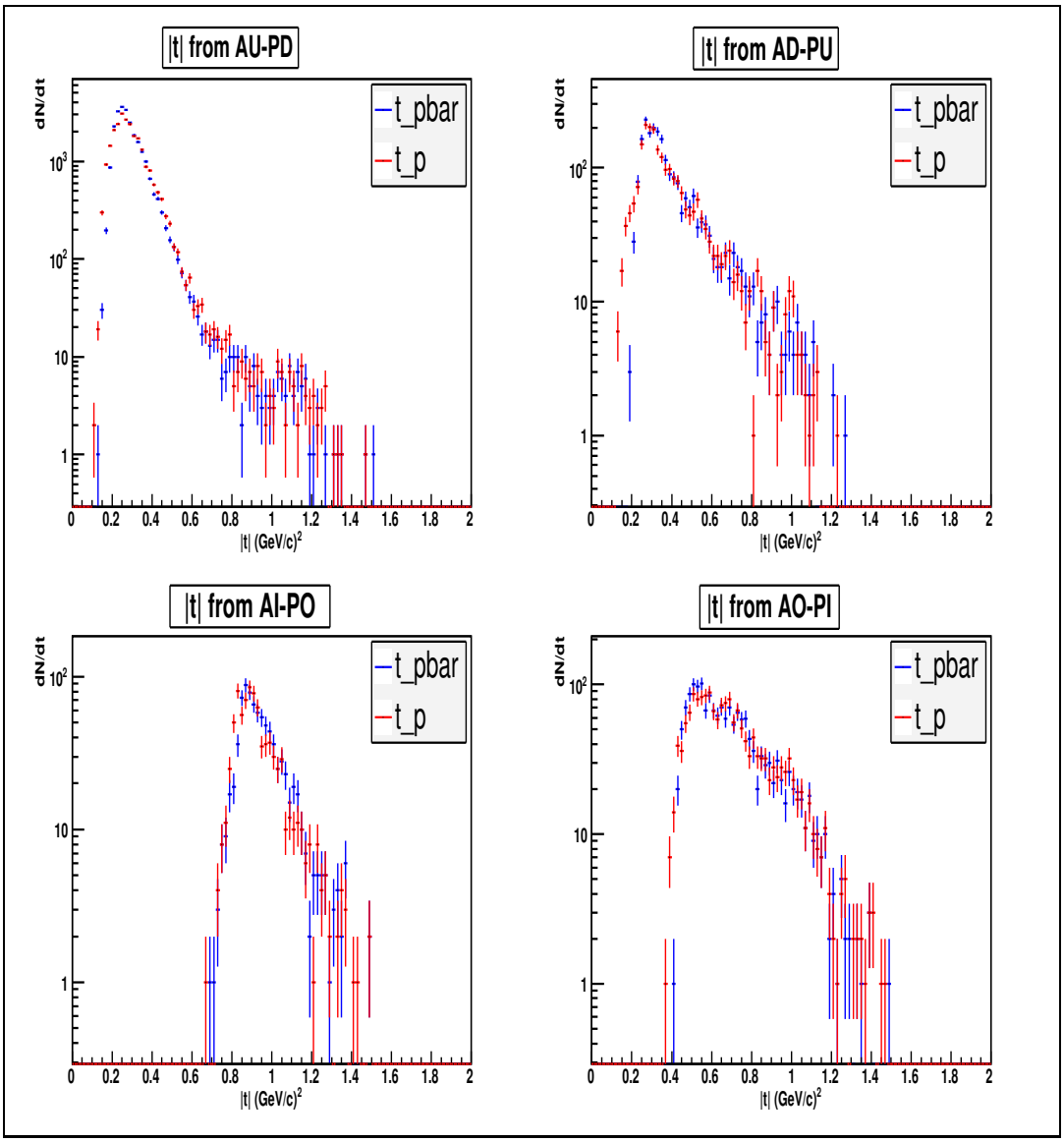

Finally we have shown in this analysis that there exist a physical elastic signal in the FPD detectors. Also this analysis allows to conclude that a good measurement of the differential cross section at center of mass energy $\sqrt{s} = 1{,}96TeV$ for t between 0.2 and 1.5 $(GeV/c)^2$ can be obtained.

Conclusions

We have made an analysis that shows that there exists an elastic signal in the FPD detectors.

It has been shown that for the data taken on February 17 and 18 of 2006 we can obtain good distributions of $\frac{dN}{dt}$ for the FPD detectors that will guarantee a correct measurement of the
differential cross section at center of mass energy $\sqrt{s} = 1{,}96TeV$ in the interval of four momentum transfer between 0.2 and 1.5 $(GeV/c)^2$

Furthermore we have obtained results for fiber efficiencies for all the scintillating fibers
belonging to the Forward Proton Detector and we have compared with other results obtained from other researchers that guarantee the good data treatment and the good results.

Recommendation

For future works and specifically for another graduate work, a good measurement can be obtained for the differential cross section at center of mass energy $\sqrt{s} = 1{,}96TeV$ in the interval of four-momentum transfer between 0.2 and 1.5 $(GeV/C)^2$ applying corrections like Background substraction, acceptance, dead fiber corrections due to effects to beam width and inefficient fibers. Also it can be inserted into the Montecarlo of elastic events future efficiency studies to obtain better corrections to the real results.

Bibliografía

[1] M. Strang *First observation of dijet events with an antiproton tag at* $\sqrt{s} = 1{,}96TeV$ *using the D∅ forward proton detector*, PhD, Thesis, The University of Texas at Arlington, 2005.

[2] C. Avila *Measurement of the proton-antiproton total cross section at center of mass energy of 1800 GeV*, PhD, Thesis, Cornell University, 1997.

[3] J. Molina, *Estudo do espalhamento elástico em colisõnes* $p\bar{p}$ *a* $\sqrt{s} = 1{,}96TeV$ *com o Detector de Prótons Frontais FPD*, Tese Doutorado, Centro Brasileiro de Pesquisas Físicas, Rio de Janeiro, Septembro de 2003.
http://www-d0.fnal.gov/results/publications_talks/thesis/date.html#2003

[4] J. Betancourt *Medicion de la sección eficaz diferencial elástica*, Tesis de Maestría, Universidad de los Andes, 2004.

[5] S. Gonzáles *Prueba de modelos difractivos en el Tevatron*, Tesis de Maestría, Universidad de los Andes, 2005.

[6] Leo W. R., *Techniques for Nuclear and Particle Physics Experiments*, Springer-Verlag, New York, (1994).

[7] F. Halzen, A. MArtin *Quarks and Leptons*, Jhon Wiley Sons, (1984).

[8] M. Block *et al*, Phys. Rev. **D 41**, 978 (1990)

[9] J. Villamil, *Mediciones de dispersión elástica con el detector FPD en el experimento* $D\emptyset$, Proyecto de grado para optar al titulo de Físico, Universidad de los Andes, 2002.

[10] M. Martens , "Coordinate System and Naming Conventions for the FPD Roman Pots", http://www-d0.fnal.gov/fpd/Links/docs.html#early/

[11] N. Amos *et al*, Phys. Rev. lett **68**, 2433 (1992).

[12] The $D\emptyset$ Collaboration, *Proposal for a Forward Proton Detector at* $D\emptyset$, Fermilab-Pub-97-377, 1997.
http://www-d0.fnal.gov/fpd/Links/docs.html#early/

[13] G. Jackson(Editor) , The Fermilab Recycler Ring Technical Design Report: Fermilab-TM-1991;
J. Thompson, Introduction to Colling Beams at Fermilab, Fermilab-TM-1904(1994).

[14] The Fermilab Run II Upgrade Committe,*The Run II Luminosity Upgrade, at Fermilab Tevatrón, submetted to the U.S. Departament of Energy.*
http://www-bd.fnal.gov/d0ereview03/docs/0verview7.1.pdf(2003)

[15] The $D\emptyset$ Collaboration, " $D\emptyset$ Run IIB Upgrade Technical Design Report" FERMILAB-PUB-02-327-E, 2002.

[16] The $D\emptyset$ Collaboration, "The $D\emptyset$ Upgrade Central Fiber Tracker: Technical Design Report". http://d0server1.fnal.gov/projects/SciFi/cft_home.html

[17] J. Barreto, "Detector Identification in the FPD system", http://www-d0.fnal.gov/fpd/Links/docs.html#early/

[18] Oguri et al, "The C++ FPD Reconstruction Code". http://alpha1.lafex.cbpf/ molina/docs/FPD_reco.ps

[19] J. Barreto and A. Drozdhin *Reconstructing Track Trajectories for the FPD*, $D\emptyset$ Note 3788, 2000.

[20] M. Martens, "Model Electrostatic Separator", http://www-d0.fnal.gov/fpd/Links/docs.html#early/

[21] R. Brun and F. Rademakers, "Reference Manual, ROOT User's Guide 5.0" http://root.cern.ch

[22] C. Avila, "fpd elastic-status report" http://www-d0.fnal.gov/fpd/Links/docs.html#elastic

[23] C. Medina, *Estudio de Montecarlo de la Resolución Espacial del Detector FPD en el Experimento* $D\emptyset$, Tesis de pregrado, Universidad de los Andes, del 2005.

[24] P. Collins, *An Introduction to Regge Theory and High Energy Physics*, Cambridge University Press, April 28 (1977).